Research Square

Preprints are preliminary reports that have not undergone peer review.
They should not be considered conclusive, used to inform clinical practice,
or referenced by the media as validated information.

Cross-Coupled Active Disturbance Rejection Synchronization Control of Load-Side Heterogeneous Dual Hydraulic Cylinders for a Temporary Support Device

Zhangxuan Ning
Shanxi Datong University
Qingsong Yao
184358338530163.com

Shanxi Datong University
Donghui Yang
Shanxi Datong University
Wencai Wang
Inner Mongolia University of Science and Technology
Xiaokun Zhao
Shanxi Datong University

Article

Keywords: temporary support device, heterogeneous dual hydraulic cylinders, synchronization control, linear active disturbance rejection control, cross-coupling control, improved particle swarm optimization

Posted Date: July 31st, 2026

DOI: https://doi.org/10.21203/rs.3.rs-10290955/v1

License: This work is licensed under a Creative Commons Attribution 4.0 International License.
Read Full License

Additional Declarations: No competing interests reported.

Cross-Coupled Active Disturbance Rejection Synchronization Control of Load-Side Heterogeneous Dual Hydraulic Cylinders for a Temporary Support Device

Zhangxuan Ning[1,3], Qingsong Yao[1*], Donghui Yang[1,3], Wencai Wang [2], Xiaokun Zhao [1, 3]

[1] Shanxi Datong University, Datong 037000, China;

[2] School of Mining and Coal, Inner Mongolia University of Science and Technology, Baotou 014010, China;

[3] The Cultivation Base of Shanxi Key Laboratory of Coal Mine Water Jet Technology and Equipment, Datong 037000, China

[*]Correspondence: 18435833853@163.com

Abstract: To address the displacement asynchronization problem of dual hydraulic cylinders caused by differences in the left and right load transfer paths, connection flexibility, and contact states during the advancing process of a temporary support device in an excavation roadway, a synchronization control model of load-side heterogeneous dual hydraulic cylinders is constructed, and a coordinated advancing control method for dual cylinders under load-side heterogeneous conditions is studied. Based on the AMESim/Simulink co-simulation platform, the load-side heterogeneous characteristics during the advancing process of the temporary support device are characterized by the differences in equivalent resistance and comprehensive flexible stiffness on the left and right load sides, and a simulation model of a heterogeneous dual-cylinder hydraulic system is established. To improve the displacement tracking performance of a single cylinder and the synchronization accuracy of dual cylinders, a LADRC+CCC synchronization control structure with asymmetric left and right parameters is constructed. The independent LADRCs on the left and right sides are used to estimate and compensate for the total disturbance of their respective channels, and the displacement synchronization error feedback of the dual cylinders is introduced through the cross-coupling link. To address the problem that empirical tuning is difficult to simultaneously consider tracking performance, synchronization accuracy, and valve-controlled input constraints, an IPSO oriented to synchronization error constraints is adopted to jointly tune the left and right controller bandwidths, observer bandwidths, nominal gains of input channels, and cross-coupling gain. The simulation results show that IPSO-LADRC+CCC exhibits good synchronization error suppression ability under the conditions of no-disturbance step input, sensor disturbance, unilateral load abrupt-change disturbance, and valve-controlled input gain attenuation. Under the no-disturbance step condition, the maximum synchronization error is 6.503×10^{-3} m, corresponding to 0.813% of the target stroke. The research results can provide a reference for the coordinated

advancing control of dual hydraulic cylinders of temporary support devices under load-side heterogeneous conditions.

Keywords: temporary support device; heterogeneous dual hydraulic cylinders; synchronization control; linear active disturbance rejection control; cross-coupling control; improved particle swarm optimization

Introduction

With the development of coal mine roadway excavation equipment toward continuity, intelligence, and reduced manpower, temporary support devices play an important role in ensuring roof stability, improving excavation efficiency, and reducing operational risks. During the advancing process, temporary support devices usually rely on the left and right dual hydraulic cylinders to cooperatively drive the support frame forward, and the displacement synchronization of the dual cylinders directly affects the posture stability and support reliability of the support frame. When the displacement responses of the left and right hydraulic cylinders are inconsistent, the support frame group is prone to deflection, torsion, local jamming, and even structural impact, thereby affecting advancing accuracy and equipment safety. Different from an ideal symmetric dual-cylinder system, the temporary support device is affected by factors such as the contact states of the roadway roof and floor, mechanism connection clearance, load transfer paths, local component deformation, and contact compression during the actual advancing process. Even if the left and right hydraulic cylinder bodies, servo valves, basic hydraulic circuits, and equivalent masses remain consistent, differences in load-side equivalent resistance and comprehensive flexible stiffness may still lead to inconsistent dynamic responses on the two sides. Therefore, studying the displacement synchronization control method of dual hydraulic cylinders under load-side heterogeneous conditions is of great significance for improving the coordinated advancing performance of temporary support devices.

In recent years, hydraulic synchronization control, electro-hydraulic servo robust control, and intelligent optimization tuning have become important research directions in the field of hydraulic equipment control. Li et al. systematically reviewed the development of hydraulic synchronization control systems and pointed out that equal-quantity synchronization, master-slave synchronization, and cross-coupled synchronization are typical closed-loop synchronization control structures. PID, fuzzy control, sliding mode control, robust control, neural networks, and intelligent optimization algorithms have all been used for synchronization error suppression [1]. For the hydraulic synchronization control problem of dual cylinders or multiple cylinders, existing studies have respectively adopted methods such as decoupled adaptive sliding mode control, ADRC-IPSO synchronization control, and cross-coupled sliding mode control to improve the synchronization performance of systems such as hydraulic supports, excavating-bolting-supporting robots, and double-lifting-point hydraulic hoists [2-4]. In heavy-duty hydraulic equipment such as hydraulic

support advancing mechanisms, multi-cylinder hydraulic supports, shield segment erectors, multi-cylinder leveling systems, aerial building machines, and hydraulic press slide leveling systems, methods such as sliding mode control, neural-network compensation, adaptive robust control, deep reinforcement learning, and cross-coupling control have also been used to improve multi-actuator coordinated motion accuracy and disturbance rejection ability [5-10]. In addition, methods such as particle swarm fuzzy PID and RBF-network adaptive sliding mode have been applied to hydraulic actuator synchronization control and multi-cylinder synchronization control of multidirectional forging hydraulic presses, further indicating the application value of intelligent optimization and nonlinear control in hydraulic synchronization systems [11-12]. In terms of electro-hydraulic servo system control, LADRC and ADRC-related methods have been widely used for objects such as electro-hydraulic position servo, unknown dead-zone compensation, high-order electro-hydraulic servo systems, independent metering electro-hydraulic systems, and low-order disturbance compensation control, because they can uniformly attribute model uncertainty, nonlinearity, and external disturbances to the total disturbance and estimate it online [13-18]. Meanwhile, methods such as particle swarm optimization, grey wolf optimization, reinforcement learning, adaptive robust control, sliding mode control, and extended state observers have also been used for parameter identification, controller tuning, and trajectory tracking control of electro-hydraulic actuators, so as to reduce the influence of empirical tuning on control performance [19-24]. The above studies show that cross-coupling, sliding mode control, ADRC, robust control, and intelligent optimization algorithms can effectively improve the synchronization accuracy and disturbance suppression ability of hydraulic systems. However, existing studies mostly focus on pipeline differences, multi-cylinder leveling, actuator coupling, general external disturbances, or single-cylinder electro-hydraulic servo tracking control, and still pay insufficient attention to the synchronization problem of dual hydraulic cylinders in which “the left and right hydraulic actuating elements and equivalent masses are consistent, while the heterogeneity mainly comes from differences in load-side resistance and flexible stiffness.”

Based on the above analysis, the advancing dual hydraulic cylinders of a temporary support device in an excavation roadway are taken as the research object, and the displacement synchronization control problem of dual cylinders under inconsistent load-side parameters is mainly studied. To address the inconsistent dynamic responses caused by differences in the left and right load transfer paths, connection flexibility, and contact states during the actual advancing process, the heterogeneous characteristics of the dual-cylinder system are characterized by the differences in load-side equivalent resistance and comprehensive flexible stiffness, and an AMESim/Simulink co-simulation model is established. On this basis, a LADRC+CCC synchronization control structure with asymmetric left and right parameters is constructed. Independent LADRCs are used to compensate for the total disturbances of the left and right channels, and dual-cylinder synchronization error feedback is introduced through cross-coupling compensation. Meanwhile, an

IPSO oriented to synchronization error constraints is adopted to jointly tune the left and right controller parameters and the cross-coupling gain, so as to reduce the influence of empirical tuning on synchronization control performance. Finally, the synchronization control performance of the proposed method in the load-side heterogeneous dual hydraulic cylinder system is verified under working conditions including no-disturbance step input, sensor disturbance, valve-controlled input gain attenuation, and unilateral load abrupt change.

1 Temporary Support Device and Hydraulic System Model

1.1 Temporary Support Device

The overall structure of the temporary support device for an excavation roadway is shown in Fig. 1. The overall structure consists of four portal support frames, guide rods, lateral pushing hydraulic cylinders, side guard plates, column shoes, forepoling beams, support beams, and other components.

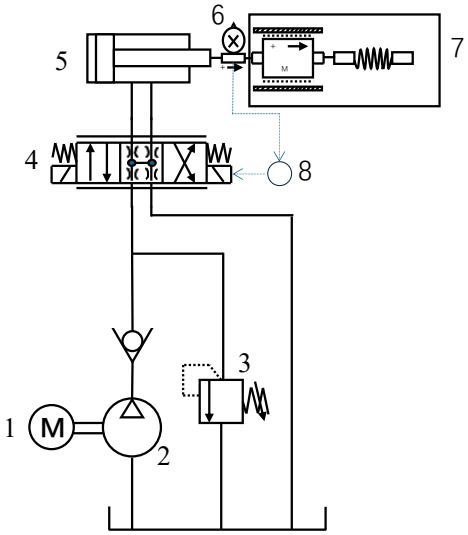


Fig. 1 Overall structure of the temporary support device

During the excavation operation, this device is used to provide temporary support for the roadway roof. The overall device is divided into odd-numbered and even-numbered portal support frames. After the roadheader completes cutting for a certain distance and stops, the even-numbered support frames first retract the side guard plates and contract the columns. Then, the lateral pushing hydraulic cylinders extend and push the even-numbered support frames forward to the specified position. After the support frames are in place, the columns extend again and the supporting state of the side guard plates is restored. Afterwards, the odd-numbered support frames complete the forward movement process in the same way. Through the alternating actions of the odd-numbered and even-numbered support frames, the continuity of the supporting function during the advance of the roadheader can be ensured.

1.2 Heterogeneous Dual-Hydraulic-Cylinder Hydraulic System of the Temporary Support Device

To address the synchronization control problem of dual hydraulic cylinders during the advancing process of the temporary support device, a schematic diagram of the load-side heterogeneous dual-hydraulic-cylinder hydraulic system of the temporary support device is established, as shown in Fig. 2. The system mainly consists of an electric motor, a hydraulic pump, a relief valve, an electro-hydraulic servo valve, hydraulic cylinders, displacement sensors, load simulation branches, and a co-simulation interface. The electric motor drives the hydraulic pump to supply oil to the system. The relief valve is used to limit the maximum working pressure of the system. The electro-hydraulic servo valve adjusts the valve port opening according to the controller output signal, thereby controlling the motion of the hydraulic cylinders on the left and right sides. The displacement sensors collect the displacements of the left and right hydraulic cylinders in real time and feed them back to the Simulink controller through the co-simulation interface, forming a displacement closed-loop synchronization control system for the dual hydraulic cylinders.



1-Electric motor；2-Hydraulic pump；3-Relief valve；4-Servo valve
5-Hydraulic cylinder；6-Displacement sensor；7-Simulated branch resistance and flexibility factors；8-Co-simulation interface

Fig. 2 Schematic diagram of the load-side heterogeneous dual-hydraulic-cylinder hydraulic system of the temporary support device

Under ideal conditions, the left and right branches of the dual-hydraulic-cylinder hydraulic system of the temporary support device are structurally symmetric and have consistent parameters, and the hydraulic cylinders on the two sides should have basically consistent dynamic responses under the same input conditions. However, during the actual advancing process, differences exist in the connection structures, load transfer paths, local component deformation, and contact compression states of the left and right support mechanisms. These differences can easily cause the left and right hydraulic cylinders to be subjected to different equivalent resistance and flexible

restoring force, thereby generating dual-cylinder synchronization errors. To characterize the above engineering asymmetric factors, the parameters of the left and right hydraulic cylinder bodies, servo valves, and basic hydraulic circuits are kept consistent in the AMESim model, and different resistance and spring parameters are set only in the load simulation branches at the rear ends of the rod chambers of the left and right hydraulic cylinders. Among them, the resistance elements are used to simulate the equivalent motion resistance in the left and right load transfer paths, the mass blocks are used to characterize the equivalent inertia of the advancing components, and the springs are used to characterize comprehensive flexible factors such as connection structure flexibility, local component deformation, and contact compression. Thus, a load-side heterogeneous dual-hydraulic-cylinder synchronization control object is constructed to study the dual-cylinder asynchronization problem caused by load-side parameter differences during the advancing process of the temporary support device.

1.3 Dynamic Model of Heterogeneous Dual Cylinders for Synchronization Control

o further clarify the dynamic characteristics of the load-side heterogeneous dual-hydraulic-cylinder hydraulic system of the temporary support device and provide a model basis for the design of the LADRC synchronization controller, a servo-valve–hydraulic-cylinder–load coupled dynamic model oriented to synchronization control is established based on the hydraulic system schematic model. The hydraulic cylinders on the left and right sides are denoted by the subscript i = L, R, respectively. The displacement, velocity, and acceleration of the hydraulic cylinder are denoted by x、$\dot{x}$、$\ddot{x}$, respectively; the pressures of the rodless chamber and rod chamber are denoted by p_{1i} and p_{2i}, respectively; the effective acting areas of the two chambers are denoted by A_1 and A_2, respectively; and the servo valve control input is denoted by u_i.

The parameters of the left and right hydraulic cylinder bodies, servo valves, and basic hydraulic circuits are consistent, namely：

$$K_{qL} = K_{qR} = K_q, K_{cL} = K_{cR} = K_c \tag{1}$$

where K_q is the servo valve flow gain, and K_c is the flow-pressure coefficient. The flow characteristics of the servo valve are linearized near the rated operating point, and the valve-port flow expression of the hydraulic cylinder on side i can be obtained as:

$$Q_{1i} = K_q u_i - K_c(p_{1i} - p_{2i}) \tag{2}$$

$$Q_{2i} = K_q u_i + K_c(p_{1i} - p_{2i}) \tag{3}$$

Where Q_{1i} and Q_{2i} are the inlet flow rate of the rodless chamber and the outlet flow rate of the rod chamber, respectively.

Considering the effects of oil compressibility, changes in hydraulic cylinder chamber volume, and equivalent internal leakage, the pressure dynamic equations of the two chambers of the hydraulic cylinder can be expressed as:

$$\dot{p}_{1i} = \frac{\beta_e}{V_{1i}}[Q_{1i} - A_1\dot{x}_i - C_t(p_{1i} - p_{2i})] \tag{4}$$

$$\dot{p}_{2i} = \frac{\beta_e}{V_{2i}}[A_2\dot{x}_i - Q_{2i} + + C_t(p_{1i} - p_{2i})] \tag{5}$$

Where β_e is the equivalent bulk modulus of the oil, C_t is the equivalent internal leakage coefficient of the hydraulic cylinder, and V_{1i} and V_{2i} are the effective volumes of the rodless chamber and rod chamber, respectively. When the extension direction of the hydraulic cylinder is taken as the positive direction, the effective volumes of the two chambers can be expressed as:

$$V_{1i} = V_{10} + A_1 x_i \tag{6}$$

$$V_{2i} = V_{20} - A_2 x_i \tag{7}$$

Where V_{10} and V_{20} are the initial volumes of the rodless chamber and rod chamber of the hydraulic cylinder, respectively. It can be seen from Eqs. (4) - (7) that changes in hydraulic cylinder displacement cause changes in chamber volume, thereby affecting the pressure dynamic process of the two chambers.

The force balance equation of the hydraulic cylinder piston and its equivalent load can be expressed as:

$$m_i\ddot{x}_i = A_1 p_{1i} - A_2 p_{2i} - B_i\dot{x}_i - F_{fi}(\dot{x}_i) - F_{ri} - k_i(x_i - x_{0i}) - F_{ci}(x_L, x_R, t) + d_i(t) \tag{8}$$

Where m_i is the equivalent mass of the hydraulic cylinder and load simulation branch on side i, B_i is the equivalent viscous damping coefficient, $F_{fi}(\dot{x}_i)$ is the friction force, F_{ri} is the equivalent resistance of the load simulation branch on side i, k_i is the comprehensive flexible stiffness on side i, x_{0i} is the displacement corresponding to the initial deformation of the spring, $F_{ci}(x_L, x_R, t)$ is the coupled load term generated when the left and right hydraulic cylinders jointly push the same support frame group, and $d_i(t)$ is the external disturbance and unmodeled dynamic term.

To simulate the differences in the left and right connection structures, load transfer paths, local

component deformation, and contact compression states during the actual advancing process of the temporary support device, the hydraulic cylinder bodies, servo valves, basic hydraulic circuits, and equivalent masses on the left and right sides are kept consistent in the AMESim model, namely:

$$mL = mR = m \tag{9}$$

The heterogeneity is constructed only through differences in the equivalent resistance and comprehensive flexible stiffness in the load simulation branches at the rear ends of the rod chambers of the left and right hydraulic cylinders, namely:

$$F_{rL} \neq F_{rR}, k_L \neq k_R \tag{10}$$

In the equation, the equivalent resistances of the left and right load simulation branches are set to 7000 N and 4000 N, respectively, and the comprehensive flexible stiffnesses of the left and right sides are set to 80000 N/m and 40000 N/m, respectively. The above parameters are used to construct the load-side heterogeneous benchmark working condition, so as to characterize the influence of differences in the load transfer paths, connection flexibility, local component deformation, and contact compression states of the left and right support mechanisms on the dynamic responses of the dual cylinders during the advancing process of the temporary support device. Among them, the equivalent resistance mainly reflects the comprehensive motion resistance formed by factors such as guide friction, contact friction, local jamming, and load transfer obstruction; the comprehensive flexible stiffness mainly reflects the equivalent elastic restoring effect formed by factors such as connection component deformation, guide mechanism flexibility, contact surface compression, and local structural constraints.

The above differences in load-side resistance and comprehensive flexible stiffness cause the left and right hydraulic cylinders to be subjected to different equivalent motion resistance and flexible restoring force under the same control input, thereby leading to inconsistent pressure responses, velocity responses, and displacement responses of the hydraulic cylinders on the two sides. When the displacement difference between the left and right cylinders increases, the support frame group is prone to deflection and torsion tendencies. Therefore, a synchronization control strategy needs to be introduced to suppress the relative displacement error of the dual cylinders.

By synthesizing Eqs. (2) - (8), it can be seen that the dual-hydraulic-cylinder hydraulic system of the temporary support device has characteristics such as pressure-flow coupling, load-side asymmetry, friction nonlinearity, and external disturbances. For the hydraulic cylinder on side i, the above complex dynamic relationship can be equivalently arranged into a second-order form oriented to LADRC design:

$$\ddot{x}_i = f_i(x_i, \dot{x}_i, p_{1i}, p_{2i}, x_L, x_R, t) + b_{0i}u_i \tag{11}$$

Where b_{0i} is the nominal control gain of the input channel of the hydraulic cylinder on side

i, and $f_i(\cdot)$ is the total disturbance term of the system, including factors such as pressure-flow coupling, friction, leakage, load-side resistance differences, spring stiffness differences, dual-cylinder coupled load, and external disturbances. Since the resistance and flexible stiffness of the left and right branches are different, generally:

$$f_L(\cdot) \neq f_R(\cdot), b_{0L} \neq b_{0R} \tag{12}$$

Therefore, the advancing hydraulic system of the temporary support device can be regarded as a dual-input dual-output hydraulic actuation system with heterogeneous characteristics. The LADRC controller does not depend on an accurate model of the controlled object. Instead, it estimates $f_i(\cdot)$ in real time through a linear extended state observer and compensates for it in the control law. Based on the above equivalent model, LADRC controllers for the left and right hydraulic cylinders are designed separately in the following sections, and dual-cylinder displacement error feedback is introduced through cross-coupling control, thereby improving the synchronization control accuracy under complex disturbance conditions.

2 Design of the Cross-Coupled Active Disturbance Rejection Control (LADRC+CCC) System

The advancing dual-cylinder hydraulic system of the temporary support device has characteristics such as load-side resistance–flexibility heterogeneity, pressure-flow coupling, friction nonlinearity, and external disturbances. The parameters of a traditional PID controller are fixed, making it difficult to simultaneously consider single-cylinder tracking performance and dual-cylinder synchronization accuracy under complex disturbances and load-side asymmetric conditions. To improve the dual-cylinder synchronization control performance during the advancing process of the temporary support device, linear active disturbance rejection control, cross-coupling control, and improved particle swarm optimization are combined to construct an IPSO-LADRC+CCC dual-cylinder synchronization control system, as shown in Fig. 3.

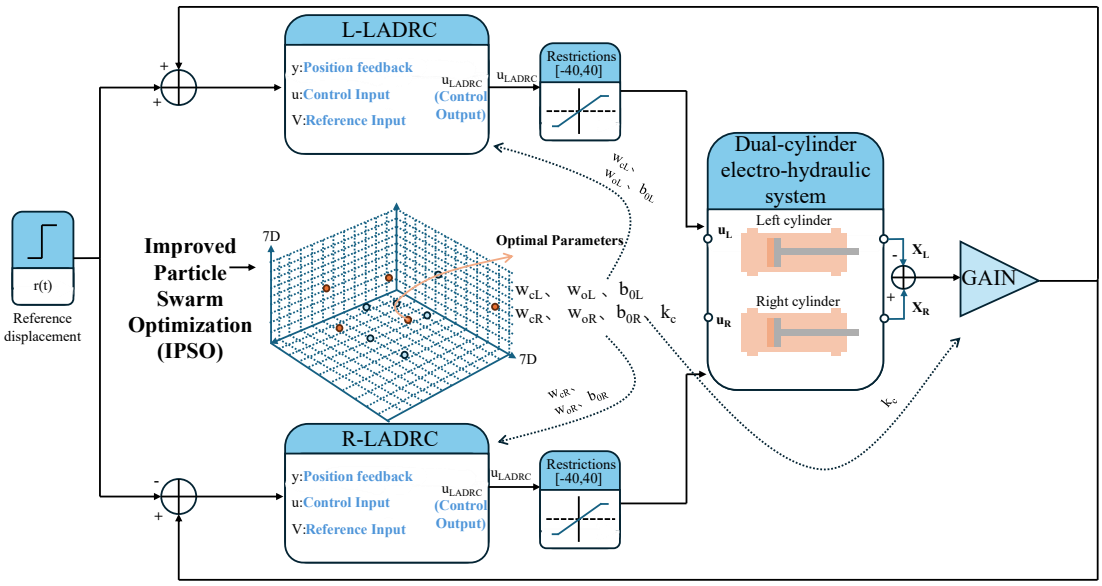


Fig. 3 Structure of the IPSO-LADRC+CCC dual-cylinder synchronization control system

The control system consists of two independent LADRC controllers on the left and right sides, a cross-coupling compensation link, a valve-controlled current limiting link, and an IPSO parameter optimization module. The left and right hydraulic cylinders each adopt an independent LADRC controller to improve the displacement tracking performance of a single cylinder. The cross-coupling compensation link constructs synchronization error feedback according to the displacement difference between the left and right cylinders, and is used to suppress the relative displacement deviation of the dual cylinders. IPSO is used to synchronously optimize the left and right LADRC parameters and the cross-coupling gain, thereby improving the synchronization control performance of the heterogeneous dual-cylinder system under complex working conditions.

2.1 Structure of the Linear Active Disturbance Rejection Controller

The linear active disturbance rejection controller uniformly attributes the unmodeled dynamics, nonlinear factors, and external disturbances in the controlled object to the total disturbance, and estimates and compensates for them in real time through an extended state observer. For the hydraulic cylinder on side i, its second-order equivalent model oriented to LADRC design can be expressed as:

$$\ddot{y}_i = f_i\left(y_i, \dot{y}_i, t\right) + b_{0i} u_i \tag{13}$$

Where $y_i\left(i = L, R\right)$ is the actual displacement of the hydraulic cylinder on side i, u_i is the servo valve control input, b_{0i} is the nominal control gain of the input channel on side i, and $f_i\left(\cdot\right)$ is the total disturbance term of the system, including factors such as load-side resistance differences, spring stiffness differences, pressure-flow coupling, friction, leakage, dual-cylinder coupled load, and external disturbances. Since the load-side parameters on the left and right sides are different,

the equivalent dynamic characteristics of the hydraulic cylinders on the two sides are different. Therefore, the parameters of the left and right LADRC controllers are set separately and optimized independently.

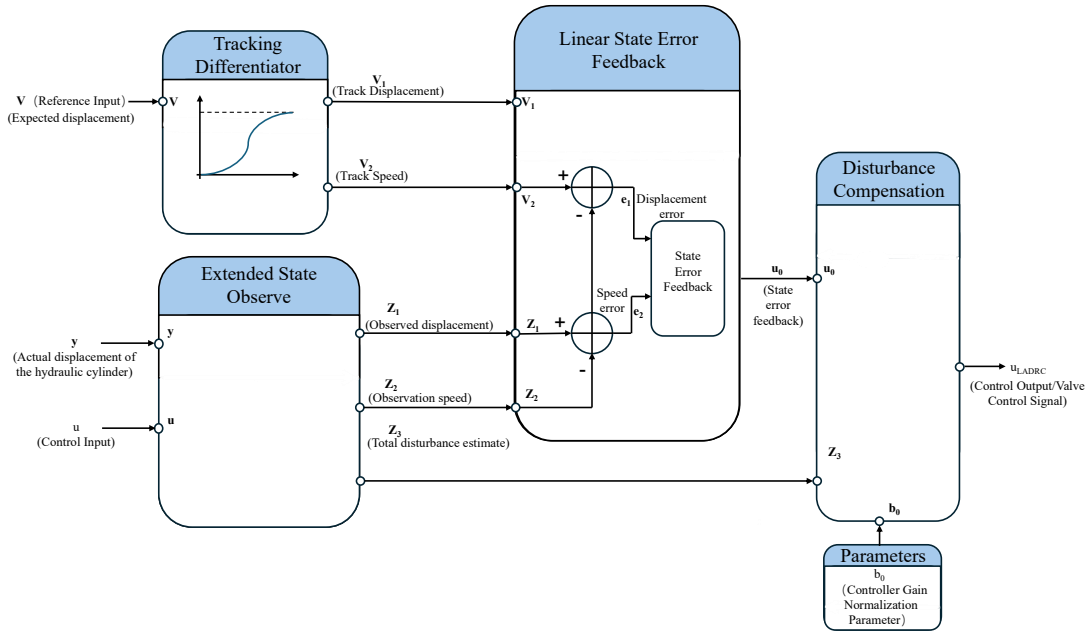


Fig. 4 Structure of the LADRC controller

2.1.1 Tracking Differentiator (TD)

To avoid an excessive instantaneous control quantity caused by the direct action of the step reference input on the controller, and to obtain smooth reference displacement and reference velocity signals, a tracking differentiator is introduced. For the given reference displacement r(k), the discrete tracking differentiator can be expressed as:

$$v_1(k+1) = v_1(k) + h \cdot v_2(k) \tag{14}$$

$$v_2(k+1) = v_2(k) + h \cdot fhan\left(v_1(k) - r(k), v_2(k), r_0, h_0\right) \tag{15}$$

Where $v_1(k)$ is the smooth tracking signal of the reference displacement, $v_2(k)$ is the reference velocity signal, h is the system integration step size, r_0 is the speed factor of the tracking differentiator, and h_0 is the filtering factor. The tracking differentiator can reduce the impact of abrupt changes in the reference input on the valve-controlled signal and improve the smoothness of the control input.

2.1.2 Linear Extended State Observer (LESO)

For the second-order object shown in Eq. (13), the extended state variables are introduced as:

$$x_{1i} = y_i, x_{2i} = \dot{y}_i, x_{3i} = f_i(\cdot) \tag{16}$$

Where x_{3i} represents the total disturbance of the system. Based on the bandwidth parameterization theory and the discretization method, a third-order discrete LESO for the hydraulic cylinder on side i is constructed [25-26]:

$$e(k) = z_1(k) - y_i(k) \tag{17}$$

$$z_{1i}(k+1) = z_{1i}(k) + h\left(z_2(k) - \beta_{1i} e_i(k)\right) \tag{18}$$

$$z_{2i}(k+1) = z_{2i}k + h\left(z_{3i}(k) - \beta_{2i} e_i(k) + b_{0i} u_i(k)\right) \tag{19}$$

$$z_{3i}(k+1) = z_{3i}(k) - h\beta_{3i} e_i(k) \tag{20}$$

Where z_{1i} and z_{2i} are the displacement and velocity of the hydraulic cylinder on side i , respectively, and z_{3i} is the observed value of the total disturbance of the system. $\beta_{1i}, \beta_{2i}\beta_{3i}$ are the observer gains of the LESO. According to the bandwidth parameterization tuning principle, an analytical relationship can be directly established between the observer gain matrix and the observer bandwidth ω_{0i}:

$$\beta_{1i} = 3\omega_{0i}, \beta_{2i} = 3{\omega_{0i}}^2, \beta_{3i} = {\omega_{0i}}^3 \tag{21}$$

2.1.3 Linear State Error Feedback (LSEF)

After the tracking differentiator outputs $v_1(k)$ and $v_2(k)$, the displacement error and velocity error of the hydraulic cylinder on side i are defined as:

$$e_{1i}(k) = v_1(k) - z_{1i}(k) \tag{22}$$

$$e_{2i}(k) = v_2(k) - z_{2i}(k) \tag{23}$$

The linear state error feedback control law is:

$$u_{0i}(k) = k_{pi} e_{1i}(k) + k_{di} e_{2i}(k) \tag{24}$$

Where k_{pi}, k_{di} are the proportional feedback gain and differential feedback gain of the LADRC on side i, respectively. Based on the controller bandwidth parameterization theory, the controller gains are expressed in terms of the controller bandwidth ω_c as follows:

$$k_{pi} = {\omega_{ci}}^2, k_{di} = 2\omega_{ci} \tag{25}$$

Where ω_{ci} is the controller bandwidth of the LADRC on side i. Using the estimated value

$z_3(k)$ of the total disturbance from the LESO, the basic control law of the LADRC on side i can be obtained as:

$$u_i(k) = \frac{u_{0i}(k) - z_{3i}(k)}{b_{0i}} \tag{26}$$

Equation (26) shows that b_{0i} directly affects the normalization of the control input and the intensity of disturbance compensation. For a load-side heterogeneous dual-cylinder system, if b_{0L} and b_{0R} adopt the same empirical value, it is easy to cause mismatched control actions of the left and right cylinders. Therefore, b_{0L} and b_{0R} are taken as parameters to be optimized and are tuned together with the controller bandwidths and observer bandwidths.

2.2 LADRC Dual-Cylinder Synchronization Control Based on Cross-Coupling

In the load-side heterogeneous dual-cylinder system, the left and right hydraulic cylinders are subjected to different equivalent motion resistance and flexible restoring force. Relying only on the independent LADRC controllers on the left and right sides can improve the single-cylinder tracking performance, but it is difficult to suppress the relative displacement error of the dual cylinders from the mechanism. Therefore, cross-coupling control is introduced based on the dual independent LADRC controllers to construct synchronization error feedback and improve the coordinated motion capability of the dual cylinders.

The reference displacement is defined as $r(t)$, and the actual displacements of the left and right hydraulic cylinders are $y_L(t)$ and $y_R(t)$, respectively. Then, the tracking errors of the left and right hydraulic cylinders are defined as:

$$e_L(t) = r(t) - y_L(t) \tag{27}$$

$$e_R(t) = r(t) - y_R(t) \tag{28}$$

The synchronization error between the dual cylinders is:

$$e_s(t) = y_R(t) - y_L(t) \tag{29}$$

To suppress the synchronization error, $e_s(t)$ is introduced into the control errors of the left and right cylinders with opposite signs, respectively, obtaining the cross-coupled comprehensive errors:

$$E_L(t) = e_L(t) + k_c \cdot e_s(t) \tag{30}$$

$$E_R(t) = e_R(t) - k_c \cdot e_s(t) \tag{31}$$

Where k_c is the cross-coupling gain, and $E_L(t)$ and $E_R(t)$ are the compensated comprehensive control errors, respectively. When the displacement of the right cylinder is greater than that of the left cylinder, that is, $e_s(t) > 0$, the comprehensive error $E_L(t)$ of the left cylinder increases, while the comprehensive error $E_R(t)$ of the right cylinder decreases. This enhances the control action of the left cylinder and weakens the control action of the right cylinder, thereby suppressing the relative displacement deviation of the dual cylinders.

In the discrete control implementation, the cross-coupling term acts on the position error feedback link of the LADRC. The velocity error of the controller on side i is still calculated from the output of the tracking differentiator and the velocity observed value of the LESO. After the introduction of cross-coupling, the LSEF of the left and right cylinders can be written as:

$$u_{0L}(k) = k_{pL} E_L(k) + k_{dL} e_{2L}(k) \tag{32}$$

$$u_{0R}(k) = k_{pR} E_R(k) + k_{dR} e_{2R}(k) \tag{33}$$

The final control laws are:

$$u_L(k) = \frac{u_{0L}(k) - z_{3L}(k)}{b_{0L}} \tag{34}$$

$$u_R(k) = \frac{u_{0R}(k) - z_{3R}(k)}{b_{0R}} \tag{35}$$

Considering the actual input current limitation of the servo valve, the controller outputs act on the electro-hydraulic servo valves after passing through the limiting links:

$$u_{Li}(k) = sat\left[u_L(k)\right] \tag{36}$$

$$u_{Ri}(k) = sat\left[u_R(k)\right] \tag{37}$$

Where $sat(\cdot)$ denotes the valve-controlled current limiting function, and the limiting range is:

$$u_{Li}, u_{Ri} \in [-40, 40]\, mA \tag{38}$$

2.3 IPSO-LADRC+CCC Optimization Method

To reduce the influence of empirical parameter tuning on synchronization control performance and improve the matching between the left and right control channel parameters and the cross-coupling compensation parameter under load-side heterogeneous conditions, an IPSO parameter

tuning method is introduced based on the LADRC+CCC control structure. The optimization variables include the controller bandwidths, observer bandwidths, nominal gains of the input channels, and cross-coupling gain of the left and right LADRC controllers. The fitness function comprehensively considers the dual-cylinder synchronization error, peak synchronization error, displacement tracking error, and valve-controlled input constraints. Through the above joint parameter tuning, a control parameter combination adapted to the differences in the left and right load characteristics can be obtained under a unified evaluation index, thereby improving the synchronization control performance of the load-side heterogeneous dual-hydraulic-cylinder system.

According to the dynamic model of load-side heterogeneous dual cylinders, although the left and right hydraulic cylinders have the same hydraulic cylinder bodies, servo valves, and basic hydraulic circuit parameters, the hydraulic cylinders on the two sides exhibit different dynamic response characteristics under the same control input because the equivalent resistance and comprehensive flexible stiffness in the load simulation branches are different. Therefore, if the left and right LADRC controllers adopt the same empirical parameters, it is difficult to simultaneously consider dual-cylinder tracking performance and synchronization accuracy. For this reason, the parameters of the left and right LADRC controllers are independently tuned, and the cross-coupling gain is incorporated into the unified optimization process. The parameter vector to be optimized for IPSO-LADRC+CCC is defined as:

$$\theta = \left[\omega_{cL}, \omega_{cR}, \omega_{oL}, \omega_{oR}, b_{0L}, b_{0R}, k_c\right] \tag{39}$$

Where ω_{cL} and ω_{cR} are the controller bandwidths of the left and right LADRC controllers, respectively; ω_{oL} and ω_{oR} are the observer bandwidths of the left and right LESOs, respectively; b_{0L} and b_{0R} are the nominal control gains of the input channels of the left and right hydraulic cylinders, respectively; and k_c is the cross-coupling gain.

The standard PSO has a simple structure and a relatively fast convergence speed, but premature convergence can easily occur in complex nonlinear optimization problems. To address the problems of strong nonlinearity of the fitness function, obvious variable coupling, and many local extrema in parameter optimization of the dual-cylinder hydraulic system, an improved particle swarm optimization algorithm is adopted. On the basis of standard PSO, IPSO introduces an adaptive weight adjustment mechanism and a stagnation disturbance mechanism to enhance the global search capability in the early stage and the local exploitation capability in the later stage of the algorithm. The flowchart of the IPSO algorithm is shown in Fig. 5.

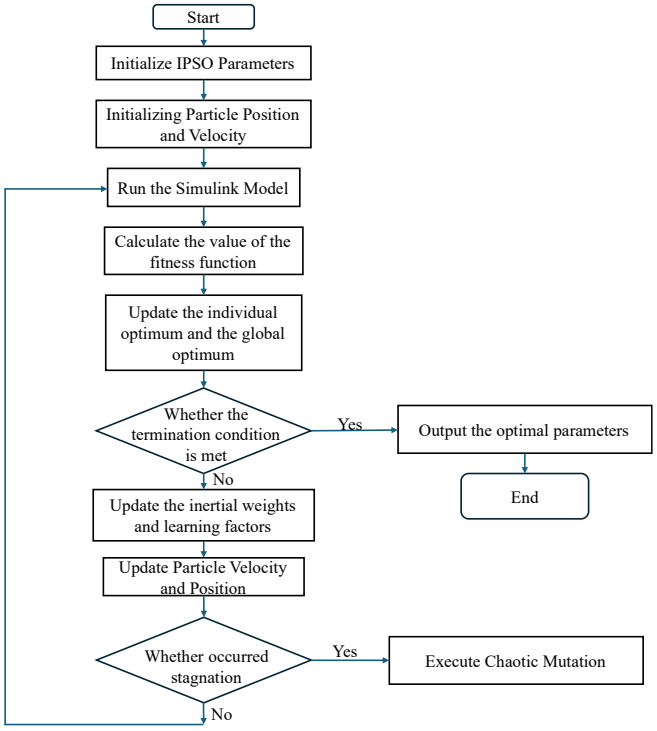


Fig. 5 Flowchart of the IPSO algorithm

The inertia weight adopts an adaptive form that decreases with the number of iterations:

$$\omega(t)=\omega_{\max}-\frac{\omega_{\max}-\omega_{\min}}{T_{\max}}t \tag{40}$$

Where $\omega_{\max},\omega_{\min}$ are the maximum and minimum values of the inertia weight, respectively, and $T_{\max}$ is the maximum number of iterations. In the early stage of optimization, $\omega(t)$ is relatively large, which is conducive to expanding the search range. In the later stage of optimization, $\omega(t)$ decreases, which is conducive to improving the local convergence accuracy.

To prevent the particle swarm from being trapped in a local optimum for a long time, a stagnation disturbance mechanism is introduced. Let the global best fitness at the k-th iteration be $F_g^{\,k}$. If the fitness value remains unchanged for N_s consecutive iterations, the particle swarm is considered to have entered a stagnation state. N_s=8. When the stagnation criterion is satisfied, random disturbance is applied to some non-optimal particles:

$$x_{i,j}^{k+1}=x_{i,j}^{k}+\eta\left(x_{j,\max}-x_{j,\min}\right)(2r-1) \tag{41}$$

Where η is the disturbance coefficient, and $r\in[0,1]$. After the disturbance, boundary constraints are imposed on the particle positions:

$$x_{i,j}^{k+1}=\min\left[\max\left(x_{i,j}^{k+1},x_{j,\min}\right),x_{j,\max}\right] \tag{42}$$

This mechanism can increase the diversity of the particle swarm while retaining the current global optimal solution, thereby improving the search capability of the algorithm in the later stage.

To further reduce the dual-cylinder synchronization error while ensuring the displacement tracking performance of the left and right hydraulic cylinders, and to avoid the valve control signal approaching the actuator saturation limit, a comprehensive fitness function composed of the synchronization error, peak error, tracking error, and valve hard-saturation penalty is constructed.

The overall evaluation term of the synchronization error is defined as:

$$J_{sync} = \frac{1}{N}\sum_{i=1}^{N}\left[\frac{e_s(t_i)}{e_0}\right]^2 \tag{43}$$

The peak synchronization error term is defined as:

$$J_{peak} = \left[\frac{\max\left|e_s(t_i)\right|}{e_0}\right]^2 \tag{44}$$

The tracking error term is defined as:

$$J_{track} = \frac{1}{2N}\sum_{i=1}^{N}\left[\left(\frac{e_L(t_i)}{r0}\right)+\left(\frac{e_R(t_i)}{r0}\right)\right]^2 \tag{45}$$

The final fitness function is $F = 0.55J_{sync} + 0.25J_{peak} + 0.20J_{track}$. In the equation, J_{sync} is used to evaluate the overall level of the synchronization error, J_{peak} is used to limit the maximum transient synchronization deviation, and J_{track} is used to ensure the tracking capability of the left and right hydraulic cylinders for the reference displacement. The total weight of the synchronization-error-related terms is 0.80, reflecting that dual-cylinder synchronization accuracy is taken as the main optimization objective. The weight of the tracking error term is 0.20, which is used to avoid weakening the overall displacement response by only reducing the relative error. The valve hard-saturation penalty term is directly superimposed on the fitness function as an actuator constraint, and is used to exclude unreasonable parameter combinations in which the control signal approaches the limiting range.

2.4 Stability and Error Boundedness Analysis

To further explain the stability basis of the designed IPSO-LADRC+CCC synchronization control system, the LESO observation error, single-cylinder tracking error, dual-cylinder synchronization error, and the influence of valve-controlled input limiting are analyzed based on the second-order LADRC equivalent model. Since the load-side heterogeneous dual-hydraulic-cylinder system of the temporary support device has characteristics such as pressure-flow coupling, load-side asymmetry, friction nonlinearity, and external disturbances, the boundedness of the closed-loop error is discussed under the conditions that the reference input, the total disturbance of the system,

and its rate of change are bounded.

For the hydraulic cylinder on side i, its LADRC design model can be expressed as:

$$y_i = f_i\left(y_i, \dot{y}_i, t\right) + b_0 u_i \tag{46}$$

Assume that $f_i(\cdot)$ and its rate of change are bounded, and $b_{0i}>0$. According to the LADRC bandwidth parameterization principle, the LESO observer gains can be expressed as:

$$\beta_{1i} = 3\omega_{0i}, \beta_{2i} = 3{\omega_{0i}}^2, \beta_{3i} = {\omega_{0i}}^3 \tag{47}$$

The corresponding characteristic polynomial of the observation error is:

$$s^3 + 3\omega_{0i}s^2 + 3{\omega_{0i}}^2 s + {\omega_{0i}}^3 = \left(s + \omega_{0i}\right)^3 \tag{48}$$

When $\omega_{0i}>0$, the observation error system is Hurwitz stable. Therefore, under the condition that the total disturbance of the system and its rate of change are bounded, the estimation errors of the LESO for displacement, velocity, and total disturbance are uniformly ultimately bounded. Increasing the observer bandwidth ω_{0i} is conducive to improving the disturbance estimation speed, but an excessively large observer bandwidth may amplify the influence of measurement noise on the control input. Therefore, the observer bandwidth is tuned within a given positive range through IPSO, so as to balance disturbance estimation capability and control input smoothness.

For the tracking error of the single-side LADRC, let:

$$e_{1i} = v_1 - Z_{1i}, \quad e_{2i} = v_2 - Z_{2i} \tag{49}$$

The linear state error feedback law is:

$$u_{0i} = k_{pi}e_{1i} + d_{di}e_{2i} \tag{50}$$

where:

$$k_{pi} = \omega_{ci}^2, \quad k_{di} = 2\omega_{ci} \tag{51}$$

In the ideal case where the observation error and input limiting residual are ignored, the single-cylinder closed-loop error dynamics can be approximately expressed as:

$$\ddot{e}_i + 2\omega_{ci}\dot{e}_i + \omega_{ci}^2 e_i = 0 \tag{52}$$

The characteristic polynomial is:

$$s^2 + 2\omega_{ci}s + \omega_{ci}^2 = (s + \omega_{ci})^2 \tag{53}$$

When $\omega_{ci} > 0$, the single-cylinder error system is stable. After considering the LESO disturbance estimation error, load-side unmodeled dynamics, and input limiting residual, the right-hand side of Eq. (52) can be regarded as a bounded residual term. Therefore, under the conditions

that the controller bandwidth satisfies $\omega_{ci} > 0$, the observation error is bounded, and the control input is bounded, the displacement tracking errors of the left and right hydraulic cylinders can both remain uniformly ultimately bounded.

According to the definitions of the tracking errors of the left and right cylinders, the synchronization error can be expressed as the difference between the left and right tracking errors. When the tracking errors of the left and right single cylinders are both uniformly ultimately bounded, the dual-cylinder synchronization error e_s is also uniformly ultimately bounded. On this basis, the cross-coupling compensation introduces the synchronization error into the left and right control channels with opposite signs:

$$E_L = e_L + k_c e_s, \quad E_R = e_R - k_c e_s \tag{54}$$

When $e_s > 0$, that is, when the displacement of the right cylinder is greater than that of the left cylinder, the comprehensive error E_L of the left cylinder increases, while the comprehensive error E_R of the right cylinder decreases. This enhances the control action of the left cylinder and weakens the control action of the right cylinder, thereby suppressing the further expansion of the synchronization error. When $e_s < 0$, the cross-coupling term produces the opposite regulating effect. Therefore, under the conditions that $k_c \geq 0$ and long-term actuator saturation is not caused, the cross-coupling compensation forms negative feedback regulation for the dual-cylinder synchronization error and does not destroy the boundedness of the single-cylinder LADRC closed-loop error.

Under local linearization conditions, the synchronization error dynamics after cross-coupling can be expressed as:

$$\ddot{e}_s + a_s \dot{e}_s + b_s e_s = \Delta_s(t) \tag{55}$$

In the equation, $a_s > 0$、$b_s > 0$ are related to the bandwidths of the left and right controllers and the cross-coupling gain, respectively; $\Delta_s(t)$ denotes the bounded term caused by differences in the left and right channel parameters, observation errors, load-side disturbances, and input limiting residuals. When $k_c \geq 0$ the controller bandwidths are positive, and $\Delta_s(t)$ is bounded, the synchronization error system is a bounded-input bounded-state system, and the dual-cylinder synchronization error e_s can remain uniformly ultimately bounded. An excessively small cross-

coupling gain weakens the synchronization error suppression capability, whereas an excessively large gain may increase the control input and induce valve-controlled limiting. Therefore, k_c is incorporated into the IPSO parameter optimization process to achieve a compromise between synchronization error suppression capability and control input constraints.

In addition, considering the actual input current limitation of the servo valve, the control input is limited within the range of [−40,40] mA. Let the limiting residual be:

$$\Delta u_i = sat(u_i) - u_i \tag{56}$$

Since $sat(\cdot)$ is a bounded function, Δu_i acts as a bounded input disturbance on the closed-loop system and can be incorporated into the total disturbance term of the system for analysis. Different from PID control with an integral link, the adopted LADRC control law does not contain an integral accumulation term. Therefore, valve-controlled input limiting does not cause the traditional integral saturation problem. However, when the control input remains at the limiting boundary for a long time, the tracking speed and synchronization accuracy of the system may decrease. To reduce long-term saturation caused by unreasonable parameter combinations, a valve-controlled input saturation penalty term is introduced into the fitness function, so that the optimization process simultaneously considers synchronization error, tracking error, and actuator input constraints.

In summary, under the conditions that the reference input, the total disturbance of the system, and its rate of change are bounded, and that $\omega_{ci} > 0, \omega_{oi} > 0, b_{oi} > 0, k_c \geq 0$, and the valve-controlled input is bounded are satisfied, the LESO observation error, single-cylinder tracking error, and dual-cylinder synchronization error can all remain uniformly ultimately bounded. Through the joint tuning of the controller bandwidths, observer bandwidths, nominal gains of the input channels, and cross-coupling gain by IPSO, combined with the valve-controlled input limiting constraint, a stability basis is provided for the synchronization control of the load-side heterogeneous dual-hydraulic-cylinder system.

3 Simulation Results

3.1 Simulation Model Construction

To verify the synchronization control effect of the synchronization control strategy and the PSO algorithm in the load-side heterogeneous dual-hydraulic-cylinder hydraulic system, co-simulation is conducted in AMESim and Simulink. According to the schematic diagram of the heterogeneous dual-hydraulic-cylinder hydraulic system, a simulation model of the heterogeneous dual-hydraulic-cylinder hydraulic system is established in AMESim, as shown in Fig. 6. To ensure the clarity of the parameter settings of the hydraulic system model, the main simulation parameters are shown in Table 1, and the control model is built in Simulink, as shown in Fig. 7.

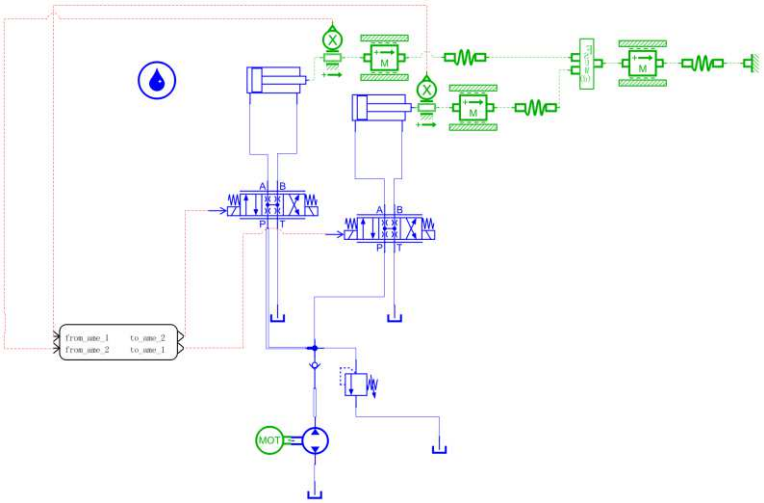


Fig. 6 AMESim simulation model of the heterogeneous dual-hydraulic-cylinder hydraulic system

To clarify the main physical parameters of the heterogeneous dual-cylinder system, the parameters of the hydraulic source, servo valve, hydraulic cylinder, oil, and load branches are summarized, as shown in Table 1. Among them, Table 1(a) gives the main basic parameters of the hydraulic system, and Table 1(b) gives the parameters representing the differences in resistance and flexible connection between the left and right branches. The asymmetric settings of the resistance and spring stiffness of the left and right branches are used to simulate the heterogeneous characteristics caused by factors such as manufacturing errors, installation deviations, connection structure deformation, and changes in contact conditions during the actual advancing process of the temporary support device.

Table 1(a) Main simulation parameters of the hydraulic system

Parameter name	Value	Unit
Hydraulic pump displacement	100	cm^3/r
Motor speed	1500	r/min
Hydraulic pump flow rate	150	L/min
Relief valve opening pressure	20	MPa
Rated current of the servo valve	40	mA
Characteristic flow rate of the servo valve	10	L/min
Corresponding pressure drop of the servo valve	5	bar
Natural frequency of the servo valve	80	Hz
Damping ratio of the servo valve	0.9	-
Hydraulic cylinder bore diameter	80	mm
Piston rod diameter	60	mm
Hydraulic cylinder stroke	0.8	m
Hydraulic cylinder dead volume	50	cm^3
Hydraulic cylinder leakage coefficient	0.001	L/(min*bar)

Table 1(b) Parameters of the heterogeneous branches

Parameter name	Left-side value	Right-side value	Unit
Branch resistance	7000	4000	N
Spring stiffness	80000	40000	N/m

To improve the clarity of the parameter settings of the simulation model and explain the engineering meanings of the load-side heterogeneous parameters, the basic parameters of the hydraulic system and the parameters of the heterogeneous branches are further described. The parameters related to the hydraulic pump, servo valve, hydraulic cylinder, and oil in Table 1(a) are used to characterize a typical valve-controlled hydraulic cylinder system for the advancing hydraulic cylinders of the temporary support device, so that the model can reflect the basic pressure-flow-displacement response relationships, such as oil supply from the hydraulic source, throttling regulation of the servo valve, extension of the hydraulic cylinder, and pressure changes in the two chambers. The resistance and spring stiffness of the left and right branches in Table 1(b) are asymmetrically set to construct a load-side heterogeneous benchmark working condition, rather than to change the structural parameters of the left and right hydraulic cylinders, servo valves, or basic hydraulic circuits themselves.

Among them, the branch resistance is used to equivalently characterize the comprehensive motion resistance formed by factors such as guide friction, contact friction, local jamming, and load transfer obstruction during the advancing process. The spring stiffness is used to equivalently characterize the comprehensive flexible restoring effect formed by factors such as deformation of support frame connectors, guide mechanism flexibility, contact surface compression, and local structural constraints. A larger resistance and stiffness are set for the left branch to simulate the condition in which one side has greater contact resistance, more obvious connection compression, or stronger local constraints during the advancing process. A relatively smaller resistance and stiffness are set for the right branch to simulate the condition in which the load transfer path on the other side is smoother or the flexible constraint is weaker.

Based on the above parameter settings, the left and right hydraulic cylinders are subjected to different load-side equivalent resistance and flexible restoring effects under the condition that the hydraulic actuating elements are consistent, thereby forming a load-side heterogeneous dual-hydraulic-cylinder simulation object with dynamic response differences. This model is mainly used to analyze the influence of load-side parameter differences on the displacement synchronization control performance of dual cylinders, and to provide a unified simulation platform for subsequent control method comparison and parameter sensitivity analysis.

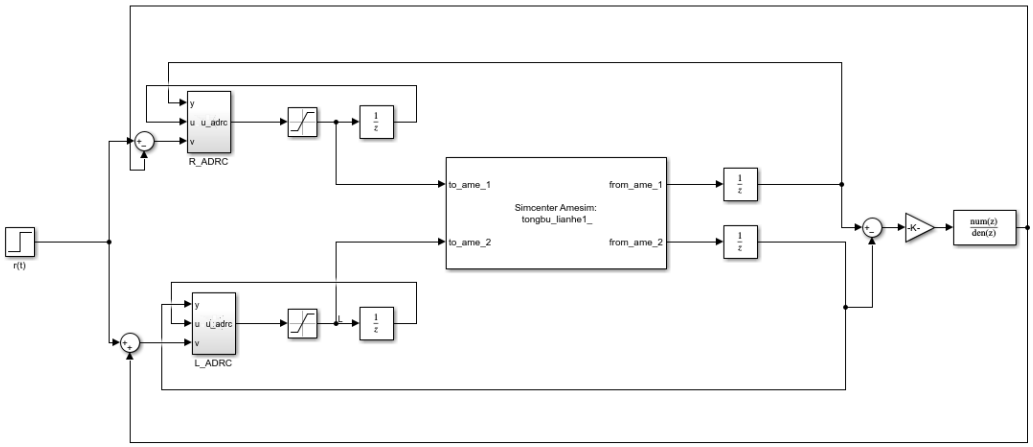


Fig. 7 Simulink dual-cylinder synchronization control model

3.2 Analysis of PSO Optimization Results

To verify the effectiveness of the improved particle swarm optimization algorithm in tuning LADRC+CCC parameters, parameter optimization and simulation comparison are conducted for PSO-LADRC+CCC, IPSO-LADRC, and IPSO-LADRC+CCC, respectively. Among them, PSO-LADRC+CCC is used to evaluate the optimization capability of the improved particle swarm optimization algorithm relative to standard PSO; IPSO-LADRC is used to analyze the influence of cross-coupling compensation on the dual-cylinder synchronization control performance; and the controller parameters are optimized as particle position vectors. For the IPSO-LADRC+CCC and PSO-LADRC+CCC control structures, the optimization variables are:

$$\theta = \left[\omega_{cL}, \omega_{cR}, \omega_{oL}, \omega_{oR}, b_{0L}, b_{0R}, k_c\right] \tag{57}$$

For IPSO-LADRC, the optimization variables are:

$$\theta = \left[\omega_{cL}, \omega_{cR}, \omega_{oL}, \omega_{oR}, b_{0L}, b_{0R}\right] \tag{58}$$

During the optimization process, the particle swarm size is set to 24, and the maximum number of iterations is set to 60. Fig. 8 shows the fitness convergence curves of PSO-LADRC+CCC, IPSO-LADRC and IPSO-LADRC+CCC.

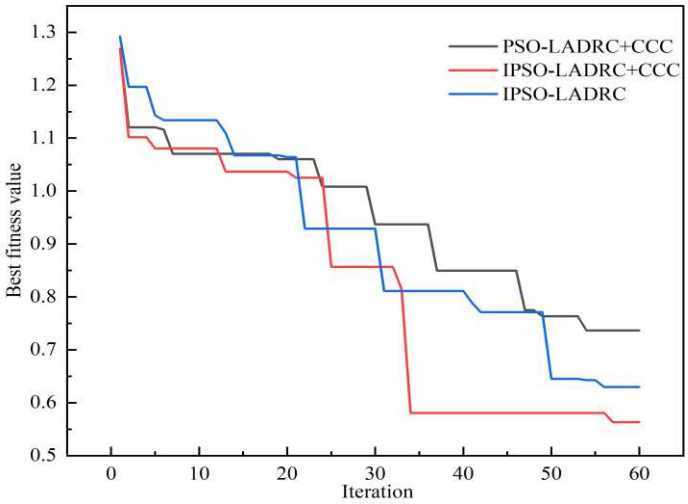


Fig. 8 Fitness convergence curves of different optimization methods

It can be seen from Fig. 8 that the fitness values of the three methods all gradually decrease with the increase in the number of iterations, indicating that particle swarm optimization can effectively complete parameter tuning of the LADRC and LADRC+CCC controllers. Compared with PSO-LADRC+CCC, IPSO-LADRC+CCC shows a faster fitness decrease rate and a lower final fitness during the optimization process, indicating that the adaptive learning factor and stagnation disturbance mechanism can improve the search performance of standard PSO and improve the parameter optimization quality of LADRC+CCC. Meanwhile, the final fitness of IPSO-LADRC+CCC is lower than that of IPSO-LADRC, indicating that under the same optimization algorithm, after cross-coupling compensation is introduced, the controller parameter combination can obtain a better comprehensive evaluation result. This shows that CCC can enhance the synchronization constraint between the left and right hydraulic cylinders, so that the optimization process not only depends on the independent adjustment of the left and right LADRC parameters, but can also further improve the coordinated performance of the dual cylinders through synchronization error feedback.

Table 2 Optimal control parameters obtained by different optimization methods

Optimization method	ω_{cL}	ω_{cR}	ω_{oL}	ω_{oR}	b_{0L}	b_{0R}	k_c
IPSO-LADRC+CCC	5.185	1.955	29.749	58.711	3.570	2.333	0.609
PSO-LADRC+CCC	5.726	2.210	38.042	51.359	4.141	2.093	0.625
IPSO-LADRC	5.270	1.287	45.447	57.559	2.834	0.981	-

It can be seen from Table 2 that the optimal control parameters of the left and right hydraulic cylinders are not completely the same, indicating that there are differences in the dynamic characteristics of the left and right channels of the load-side heterogeneous dual-hydraulic-cylinder

system. Therefore, asymmetric parameter tuning is required to compensate for the differences in load-side equivalent damping, comprehensive stiffness, and valve-controlled response characteristics on the two sides. Overall, the comparison between PSO-LADRC+CCC and IPSO-LADRC+CCC shows that IPSO can improve the search quality and convergence performance of LADRC+CCC parameter tuning. The comparison between IPSO-LADRC and IPSO-LADRC+CCC shows that cross-coupling compensation can further improve the comprehensive fitness.

3.3 Simulation Result Analysis

To verify the tracking performance and disturbance rejection ability of active disturbance rejection cross-coupling control based on improved particle swarm optimization (IPSO-LADRC+CCC), active disturbance rejection cross-coupling control based on particle swarm optimization (PSO-LADRC+CCC), active disturbance rejection control based on improved particle swarm optimization (IPSO-LADRC), traditional active disturbance rejection cross-coupling control (LADRC+CCC), and cross-coupling control based on traditional PID control in dual-hydraulic-cylinder synchronization control, four working conditions are set: no-disturbance step input, sensor disturbance, valve-controlled input gain attenuation disturbance, and unilateral load abrupt-change disturbance. The four working conditions are used to evaluate the synchronization control performance of the controllers under ideal conditions, measurement feedback-side disturbance, actuator input-side disturbance, and load-side disturbance, respectively.

To ensure the clarity and repeatability of the disturbance working condition settings, the sensor signal disturbance, unilateral load abrupt-change disturbance, and valve-controlled input gain attenuation disturbance are uniformly described. The no-disturbance step condition is used as the basic comparison condition to evaluate the displacement tracking and dual-cylinder synchronization performance of each control method under ideal conditions. The sensor signal disturbance is used to simulate measurement noise and transmission interference in the displacement feedback channel. The unilateral load abrupt-change disturbance is used to simulate a short-term additional load or local jamming impact on one hydraulic cylinder. The valve-controlled input gain attenuation disturbance is used to simulate a decrease in the output gain of the proportional valve driver or attenuation of valve-controlled current transmission. The settings of each disturbance working condition are shown in Table 3.

Table 3 Settings of disturbance working conditions

Working condition	Disturbance type	Application position	Disturbance parameter	Disturbance time
Sensor signal disturbance	Zero-mean band-limited random noise	Left and right displacement feedback channels	Standard deviation of 1.0×10^{-3} m	$t\geqslant1$s

Unilateral load abrupt-change disturbance	Rectangular-pulse additional resistance	Load end of the left hydraulic cylinder	Amplitude of 3000 N	4.35 – 5.05s
Valve-controlled input gain attenuation disturbance	Multiplicative attenuation of the input channel	Actual input end of the left servo valve	Actual valve-controlled input attenuated by 5%, the gain coefficient is 0.95	4.35 – 5.05s

The unilateral load abrupt-change disturbance and the valve-controlled input gain attenuation disturbance are both set between 4.35 s and 5.05 s. This time period is located in the interval where the hydraulic cylinder is close to the target displacement and transitions from the rapid advancing stage to the stable stage. At this time, the system has not completely entered the steady state and is relatively sensitive to load abrupt changes and input channel degradation, making it suitable for evaluating the disturbance rejection ability and post-disturbance recovery ability of the controller during the critical advancing stage. The disturbance duration is set to 0.7 s, which can form a relatively obvious transient disturbance response without changing the final reference target, thereby facilitating comparison of the synchronization error peaks and recovery processes of different control methods.

3.3.1 Performance Comparison of Heterogeneous Dual Cylinders under the No-Disturbance Step Condition

The no-disturbance step condition is used to evaluate the basic synchronization control performance of each control method. In the simulation, the target displacement is set to 0.8 m, and the reference signal steps from 0 m to 0.8 m at t=1 s. Under this condition, only the displacement response speed and dual-cylinder synchronization accuracy of different control methods under the same reference input are compared. To verify the control effects of different control systems on the synchronization of heterogeneous dual hydraulic cylinders of the temporary support device under the no-disturbance step condition, IPSO-LADRC+CCC, PSO-LADRC+CCC, IPSO-LADRC, LADRC+CCC, PID+CCC, and the open-loop system are used for comparison. The simulation results are shown in Fig. 9, Fig. 10, and Table 4.

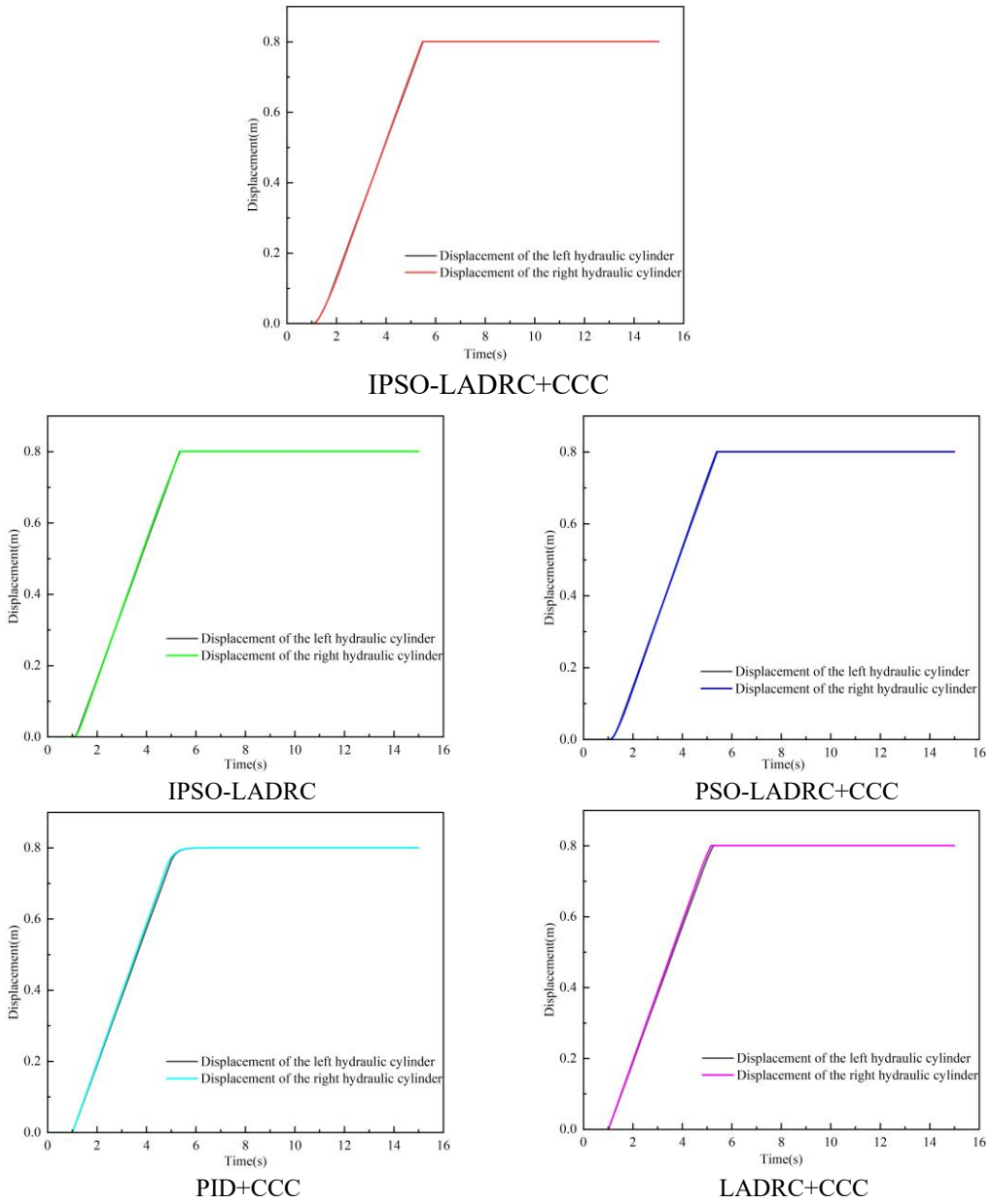


Fig. 9 Dual-cylinder displacements of different control methods under the no-disturbance step condition

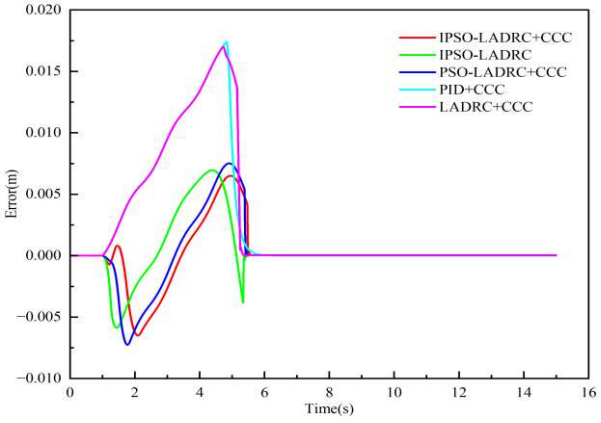


Fig. 10 Dual-cylinder errors of different control methods under the no-disturbance step condition

Table 4 Performance indices under the no-disturbance step condition

Control method	$\max\|e_{sync}\|$/m	$RMSe_{sync}$/m	$IAEe_{sync}$	First arrival time at 0.8 m	Arrival time difference between the left and right cylinders
IPSO-LADRC+CCC	0.006503	0.002292	0.015646	4.488	0.0225
IPSO-LADRC	0.006959	0.002362	0.016163	4.359	0.0233
PSO-LADRC+CCC	0.007515	0.002594	0.017867	4.409	0.0288
LADRC+CCC	0.017005	0.005826	0.039930	4.241	0.0940
PID+CCC	0.017402	0.005603	0.038086	5.356	0.0271

Among them, the first arrival time at 0.8 m and the settling time are both measured from the start of the step input. The settling time is determined by the criterion that the response enters the $0.8 \pm 2\%$ error band and remains within it without exceeding the band again.

Under the no-disturbance condition, IPSO-LADRC+CCC performs best in terms of synchronization error indices. Its maximum synchronization error, RMS synchronization error, and IAE are 6.503×10^{-3}m、2.292×10^{-3}m and 1.565×10^{-2}, respectively, all of which are lower than those of the other comparison methods. Compared with PSO-LADRC+CCC, the three indices are reduced by 13.46%, 11.66%, and 12.43%, respectively, indicating that IPSO can improve the parameter optimization quality of LADRC+CCC. Compared with IPSO-LADRC, after CCC is introduced, the maximum synchronization error, RMS synchronization error, and IAE are reduced by 6.55%, 2.98%, and 3.20%, respectively, indicating that cross-coupling compensation can further improve the synchronization performance of the dual cylinders.

Compared with LADRC+CCC and PID+CCC, the maximum synchronization error of IPSO-LADRC+CCC is reduced by 61.76% and 62.63%, respectively, and the RMS synchronization error is reduced by 60.66% and 59.10%, respectively. This indicates that the proposed method has obvious advantages in synchronization accuracy compared with unoptimized LADRC and traditional PID+CCC. Although LADRC+CCC has a shorter first arrival time at 0.8 m and settling time, its synchronization error is significantly larger than that of IPSO-LADRC+CCC, indicating that its fast response is accompanied by a relatively large dual-cylinder synchronization deviation. Overall, IPSO-LADRC+CCC does not take the fastest displacement response as its objective, but significantly reduces the synchronization error during the dual-cylinder motion process on the basis of ensuring that the system stably reaches the target displacement, making it more suitable for coordinated control of dual hydraulic cylinders with synchronization accuracy as the core objective.

3.3.2 Load-Side Parameter Sensitivity under the No-Disturbance Step Condition

To further examine the adaptability of the proposed control method to changes in load-side

parameters and to avoid the conclusion under the no-disturbance step benchmark condition depending only on a single heterogeneous parameter combination, load-side parameter sensitivity analysis is carried out based on the no-disturbance step condition by changing the equivalent resistance and comprehensive flexible stiffness of the left and right load simulation branches. Under different working conditions, only the resistance and spring stiffness of the left and right branches are changed, while the hydraulic cylinders, servo valves, hydraulic source, reference input, controller structure, and control parameters remain unchanged. The maximum synchronization error, root mean square value of the synchronization error, and synchronization error integral are adopted as evaluation indices to analyze the synchronization control performance of IPSO-LADRC+CCC under different degrees of load-side heterogeneity. The working condition settings for parameter sensitivity analysis are shown in Table 5.

Table 5 Working condition settings for load-side parameter sensitivity analysis

Working condition	Left-side resistance/N	Right-side resistance/N	Left-side stiffness/(N/m)	Right-side stiffness/(N/m)	Working condition description
S1	6000	5000	70000	50000	Mild heterogeneity
S2	7000	4000	80000	40000	Benchmark heterogeneity
S3	8000	3000	80000	40000	Increased resistance difference
S4	7000	4000	100000	30000	Increased stiffness difference
S5	8000	3000	100000	30000	Simultaneous increase in resistance and stiffness differences

The synchronization control performance under different load-side heterogeneous parameter combinations is shown in Table 6. It can be seen from the table that, under the same no-disturbance step input and the same control parameters, differences in load-side equivalent resistance and comprehensive flexible stiffness affect the synchronization error level of the dual hydraulic cylinders. Compared with the benchmark heterogeneous condition S2, the maximum synchronization error, RMS synchronization error, and IAE of the mild heterogeneous condition S1 are all reduced, indicating that when the differences between the left and right load sides decrease,

the consistency of the dual-cylinder displacement responses is improved. When the resistance difference or stiffness difference increases, the synchronization errors under conditions S3 and S4 are both higher than those under the benchmark condition, indicating that both the difference in load-side motion resistance and the difference in flexible restoring effect weaken the coordinated advancing performance of the dual cylinders. Among them, the synchronization error under the increased stiffness difference condition is slightly higher than that under the increased resistance difference condition, indicating that the difference in comprehensive flexible stiffness further affects the dual-cylinder displacement synchronization accuracy by changing the load-side elastic restoring effect.

Table 6 Synchronization control performance under different load-side heterogeneous parameters

Working condition	$\max\lvert e_{sync}\rvert$/m	$RMSe_{sync}$/m	$IAEe_{sync}$
S1	0.005421	0.001936	0.013284
S2	0.006503	0.002292	0.015646
S3	0.007286	0.002518	0.017203
S4	0.007815	0.002681	0.018126
S5	0.008936	0.003047	0.020384

Further comparison of condition S5 shows that when the resistance difference and stiffness difference between the left and right branches increase simultaneously, the dual-cylinder synchronization error reaches the highest level. This indicates that an increase in the degree of load-side heterogeneity aggravates the inconsistency in the dynamic responses of the left and right hydraulic cylinders. However, under conditions S1–S5, IPSO-LADRC+CCC can maintain a relatively low synchronization error level in all conditions, indicating that the proposed method has good adaptability within a certain range of load-side resistance and flexible stiffness variations.

In summary, under the no-disturbance step condition, differences in load-side equivalent resistance and comprehensive flexible stiffness are important factors affecting the synchronization performance of the dual hydraulic cylinders of the temporary support device. The parameter sensitivity analysis results show that the proposed IPSO-LADRC+CCC method is not only applicable to a single benchmark parameter combination, but can also maintain low synchronization errors and relatively stable control inputs under different degrees of load-side heterogeneity. This result further indicates the necessity of incorporating differences in load-side resistance and flexible stiffness into the synchronization control modeling of dual hydraulic cylinders, and also further supports the applicability of the proposed control method in coordinated advancing scenarios of temporary support devices.

3.3.3 Performance Comparison under the Sensor Disturbance Condition

The sensor signal disturbance condition is used to simulate the influence of measurement noise, sampling error, and signal transmission interference on the displacement sensors during actual operation. In the simulation, mutually independent zero-mean discrete Gaussian random noise is

added to the displacement feedback channels of the left and right hydraulic cylinders in Simulink, respectively. The noise standard deviation is1.0×10^{-3}m, and the sampling time is 0.01 s. At this time, the feedback signals received by the controller can be expressed as:

$$y_{mi}(t) = y_i(t) + n_i(t), i = L, R \tag{59}$$

Where $y_{mi}(t)$ is the displacement feedback signal after measurement noise is added, $y_i(t)$ is the actual displacement of the hydraulic cylinder, and $n_i(t)$ is the zero-mean discrete Gaussian random noise. Since both LADRC and cross-coupling control rely on displacement feedback to calculate the tracking error and synchronization error, this condition can be used to evaluate the synchronization maintenance capability of the controller under measurement feedback uncertainty. To verify the control effects of different control systems on the synchronization of heterogeneous dual hydraulic cylinders of the temporary support device under the sensor disturbance condition, IPSO-LADRC+CCC, PSO-LADRC+CCC, IPSO-LADRC, LADRC+CCC, and PID+CCC are used for comparison. The simulation results are shown in Figs. 11 and 12 and Table 7.

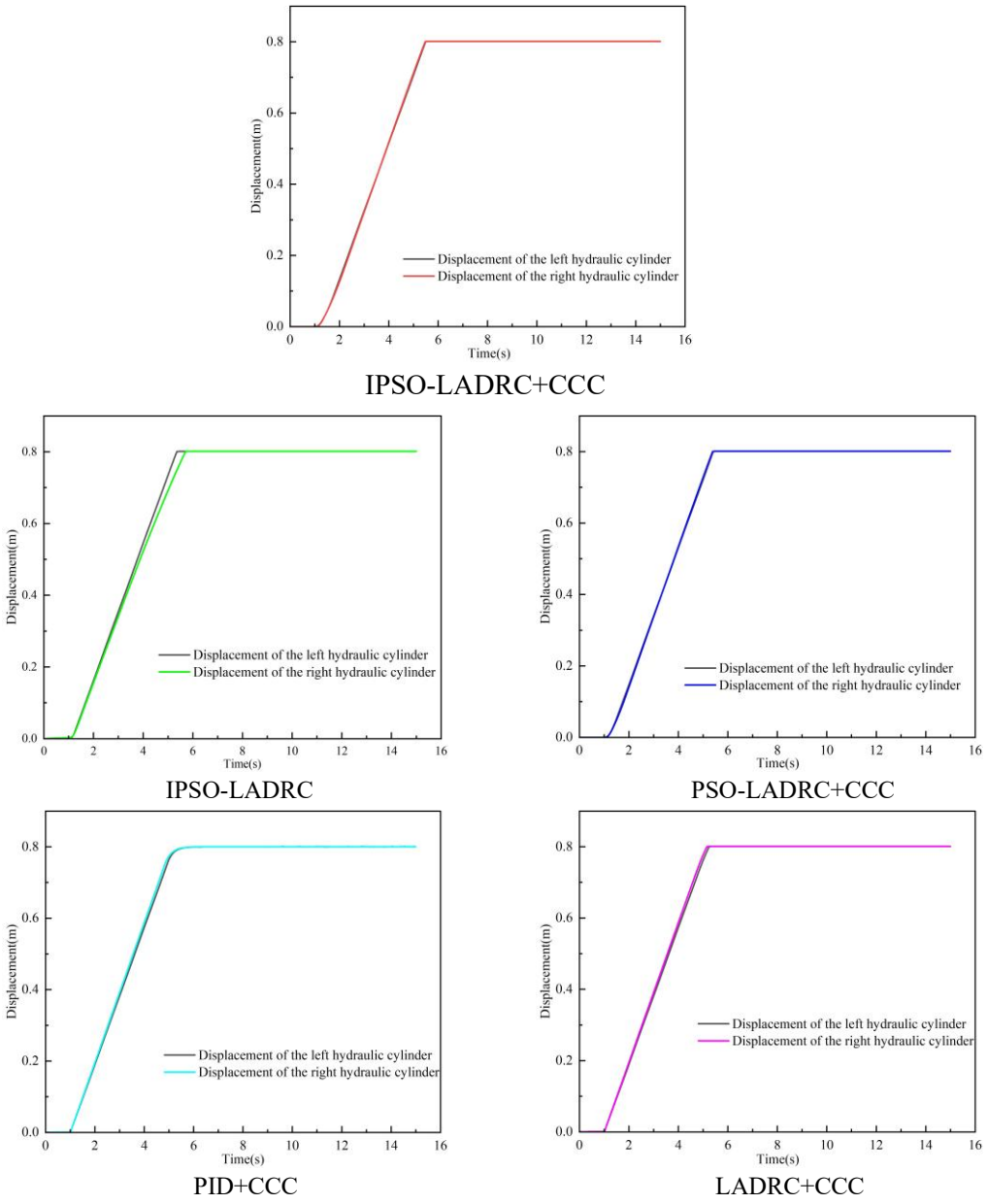


Fig. 11 Dual-cylinder displacements of different control methods under the sensor signal disturbance condition

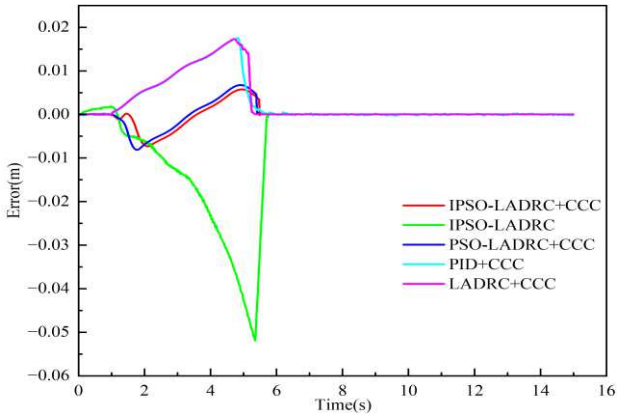


Fig. 12 Dual-cylinder errors of different control methods under the sensor signal disturbance condition

Table 7(a) Performance indices under the sensor signal disturbance condition

Control method	$\max\|e_{sync}\|$/m	$RMSe_{sync}$/m	$Stde_{sync}$/m	$P2Pe_{sync}$/m
IPSO-LADRC+CCC	0.007323	0.002312	0.002309	0.013063
PSO-LADRC+CCC	0.008121	0.002599	0.002598	0.014857
PID+CCC	0.017563	0.005693	0.004972	0.017866
LADRC+CCC	0.017312	0.005975	0.005195	0.017435
IPSO-LADRC	0.051920	0.013544	0.012015	0.053672

Where $P2Pe_{sync}$ denotes the peak-to-peak value of the synchronization error.

Table 7(b) Performance indices under the sensor signal disturbance condition

Control method	IAE_{sync}	First arrival time at 0.8 m	Arrival time difference between the left and right cylinders
IPSO-LADRC+CCC	0.015704	4.487	0.0185
PSO-LADRC+CCC	0.017996	4.408	0.0248
PID+CCC	0.039899	5.349	0.1721
LADRC+CCC	0.041320	4.238	0.0966
IPSO-LADRC	0.088750	4.697	0.3504

Under the sensor signal disturbance condition, IPSO-LADRC+CCC performs best in terms of synchronization error indices. Its maximum synchronization error, RMS synchronization error, standard deviation of the synchronization error, peak-to-peak value, and IAE are 7.323×10^{-3}m、2.312×10^{-3}m、2.309×10^{-3}m、1.306×10^{-2}m and 1.570×10^{-2}, respectively, all of which are lower than those of the other comparison methods. This indicates that the proposed method has good synchronization robustness against measurement noise.

Compared with PSO-LADRC+CCC, the maximum synchronization error, RMS synchronization error, and IAE of IPSO-LADRC+CCC are reduced by 9.83%, 11.04%, and 12.74%, respectively, indicating that IPSO can still obtain a better LADRC+CCC parameter tuning effect under sensor disturbance conditions. Compared with IPSO-LADRC, after CCC is introduced, the maximum synchronization error, RMS synchronization error, and IAE are reduced by 85.90%, 82.93%, and 82.31%, respectively, indicating that cross-coupling compensation plays a significant role in suppressing dual-cylinder synchronization deviation under sensor disturbance.

Compared with PID+CCC and LADRC+CCC, the maximum synchronization error of IPSO-LADRC+CCC is reduced by 58.30% and 57.70%, respectively, and the RMS synchronization error is reduced by 59.39% and 61.31%, respectively. Although LADRC+CCC has a shorter first arrival time at 0.8 m, its synchronization error is significantly larger than that of IPSO-LADRC+CCC. Meanwhile, IPSO-LADRC+CCC has the smallest arrival time difference between the left and right cylinders, indicating that this method can better maintain the motion coordination of the dual

cylinders under measurement disturbance. Overall, IPSO-LADRC+CCC has better synchronization accuracy and measurement noise rejection capability under the sensor disturbance condition.

3.3.4 Performance Comparison of Heterogeneous Dual Cylinders under the Unilateral Load Abrupt-Change Disturbance Condition

To simulate the situation in which one hydraulic cylinder is subjected to a sudden load, external impact, local jamming, or load imbalance during the operation of an actual dual-cylinder system, a rectangular-pulse additional resistance is applied to the load end of the left hydraulic cylinder in the AMESim hydraulic model. The disturbance force amplitude is set to 3000 N, the action time is 4.35–5.05 s, and the duration is 0.7 s. This disturbance is not directly applied to the right hydraulic cylinder. The disturbance can be expressed as:

$$\begin{aligned} F_{dL}(t) &= \begin{cases} 3000N, 4.35 \le t \le 5.05 \\ 0, \qquad other \end{cases} \\ F_{dR}(t) &= 0 \end{aligned} \tag{60}$$

Where $F_{dL}(t)$ and $F_{dR}(t)$ are the additional disturbance forces at the load ends of the left and right hydraulic cylinders, respectively. This condition increases the force difference between the left and right hydraulic cylinders within a short period of time, and is used to examine the synchronization error suppression capability and post-disturbance recovery capability of the controller under a unilateral load abrupt change. The simulation results of different control methods under this condition are shown in Fig. 13, Fig. 14, and Table 8.

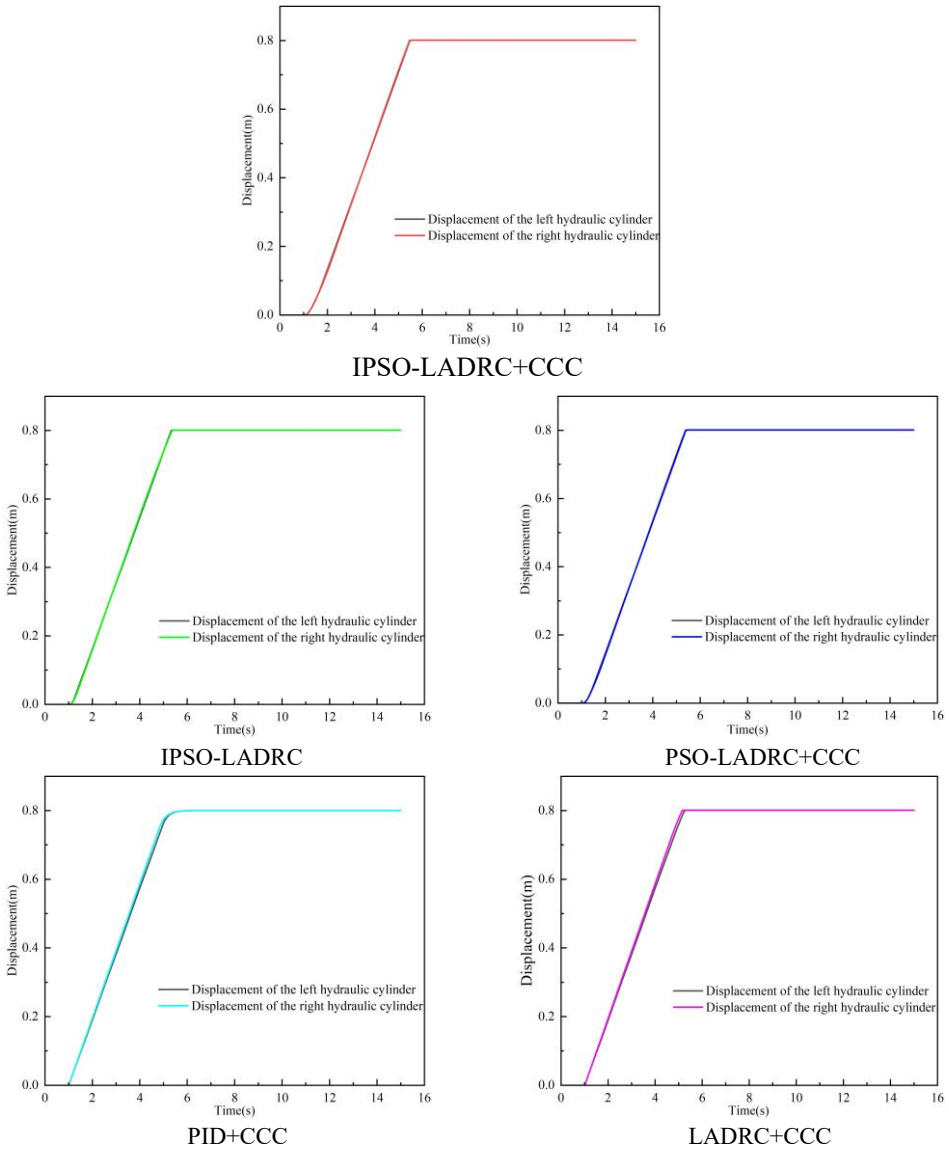


Fig. 13 Dual-cylinder displacements of different control methods under the unilateral load abrupt-change disturbance condition

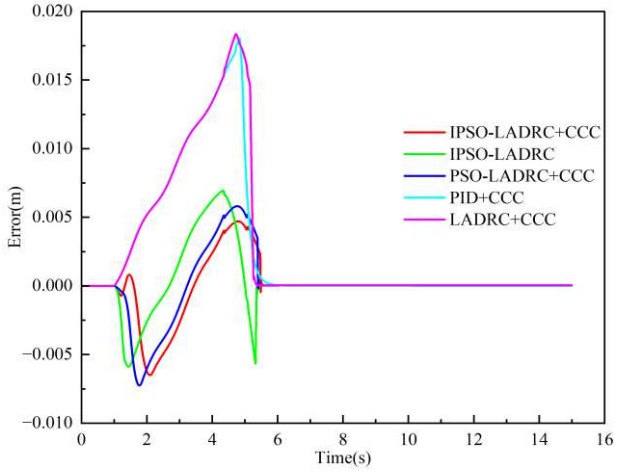


Fig. 14 Dual-cylinder errors of different control methods under the unilateral load abrupt-change disturbance condition

Table 8 Performance indices under the unilateral load abrupt-change disturbance condition

Control method	$\max\|e_{sync}\|$/m	$RMSe_{sync}$/m	IAE_{sync}	During $\max\|e_{sync}\|$/m	Recovery time/s
IPSO-LADRC+CCC	0.006499	0.002010	0.013886	0.004701	0.426
IPSO-LADRC	0.006946	0.002295	0.015767	0.006946	0.308
PSO-LADRC+CCC	0.007515	0.002594	0.017867	0.007515	0.359
PID+CCC	0.018029	0.005650	0.038431	0.018029	0.342
LADRC+CCC	0.018347	0.006010	0.040938	0.018347	0.207

It can be seen from Table 8 that under the unilateral load abrupt-change disturbance condition, IPSO-LADRC+CCC obtains the smallest synchronization error indices. Its maximum synchronization error over the whole process, RMS synchronization error, and IAE are 6.499×10^{-3} m、2.010×10^{-3} m and 1.3886×10^{-2}, respectively, all of which are lower than those of the other comparison methods. During the disturbance period, the maximum synchronization error of IPSO-LADRC+CCC is 4.701×10^{-3} m, which is also the smallest among all methods, indicating that the proposed method can effectively suppress the dual-cylinder synchronization deviation caused by the unilateral load abrupt change.

Compared with PSO-LADRC+CCC, the maximum synchronization error, RMS synchronization error, and IAE of IPSO-LADRC+CCC are reduced by 13.52%, 22.51%, and 22.28%, respectively, indicating that IPSO has a better parameter optimization effect under the unilateral load abrupt-change disturbance. Compared with IPSO-LADRC, after CCC is introduced, the three indices are reduced by 6.44%, 12.42%, and 11.93%, respectively, and the maximum synchronization error during the disturbance period is reduced by 32.32%, indicating that cross-coupling compensation can further improve the dual-cylinder synchronization performance under the unilateral load abrupt change.

Compared with LADRC+CCC and PID+CCC, the synchronization error advantage of IPSO-LADRC+CCC is more obvious. Its maximum synchronization error is reduced by 64.58% and 63.95%, respectively, and its RMS synchronization error is reduced by 66.56% and 64.42%, respectively. Although LADRC+CCC has the shortest recovery time, which is 0.207 s, its synchronization error peak is obviously larger. The recovery time of IPSO-LADRC+CCC is 0.426 s, but its error peak, RMS error, and IAE are all the smallest. Therefore, the disturbance rejection effect cannot be evaluated only according to the recovery time. Overall, IPSO-LADRC+CCC has better synchronization accuracy and disturbance rejection performance under the unilateral load abrupt-change disturbance.

3.3.5 Performance Comparison of Heterogeneous Dual Cylinders under the Valve-Controlled Input Gain Attenuation Disturbance Condition

The valve-controlled input gain attenuation disturbance is used to simulate situations such as a decrease in the output gain of the proportional valve driver, attenuation of valve-controlled current transmission, or short-term degradation of the actuator input channel. Considering that the valve-controlled currents of all control methods are constrained by the [−40,40] mA limiting range, if an additive disturbance is directly superimposed before limiting, the disturbance may be offset by the limiting link when the control signal is in the saturated state. Therefore, the disturbance is set at the actual valve-controlled input end after limiting, so as to simulate short-term gain degradation of the actual actuator input channel.

Combined with factors that may exist in engineering applications of the valve-controlled input channel, such as driver output attenuation, current transmission errors, and valve port response degradation, the actual input gain of the left servo valve is set to decrease by 5% for a short time; that is, during the disturbance period, the actual valve-controlled input is 95% of the controller output after limiting. The 5% attenuation is used to characterize mild-to-moderate actuator input channel degradation, which can introduce observable inconsistency between the left and right drives while avoiding response distortion or long-term saturation caused by excessive attenuation. The actual input current of the left servo valve is defined as:

$$I_{vL}(t) = \lambda(t) sat(iL(t)) \tag{61}$$

$$\lambda(t) = \begin{cases} 0.95, 4.35 \le t \le 5.05 \\ 1, \quad other \end{cases} \tag{62}$$

No gain attenuation is applied to the input of the right servo valve, namely:

$$I_{vR}(t) = sat(iR(t)) \tag{63}$$

Where $sat(\cdot)$ denotes the valve-controlled current limiting function, and the limiting range is [-40,40] mA. This setting indicates that the actual input of the left proportional valve undergoes short-term attenuation during the disturbance period, and is used to examine the synchronization compensation capability of the controller for uncertainty in the actuator input channel. The simulation results are shown in Figs. 15 and 16 and Table 9.

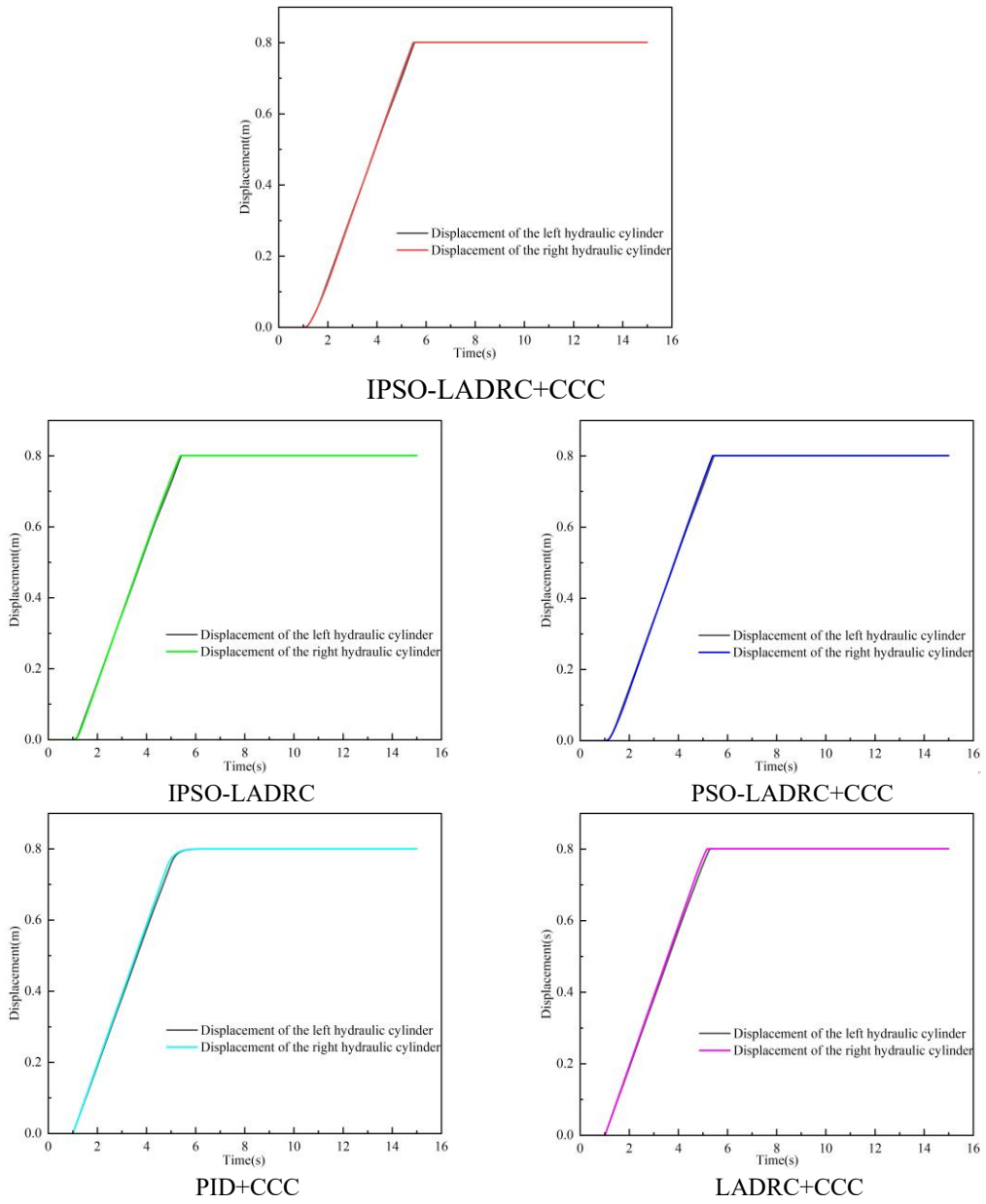


Fig. 15 Dual-cylinder displacements of different control methods under the valve-controlled input gain attenuation disturbance condition

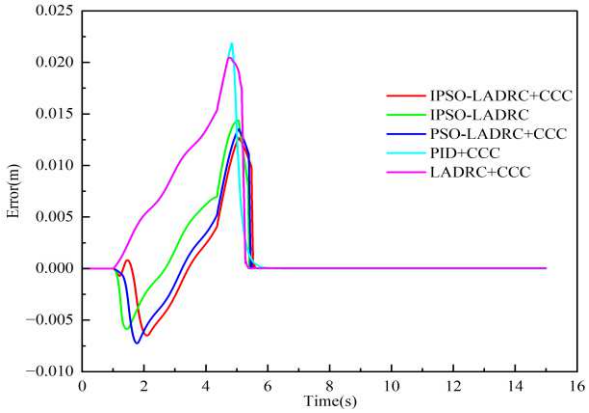


Fig. 16 Dual-cylinder errors of different control methods under the valve-controlled input gain attenuation disturbance condition

Table 9(a) Performance indices under the valve-controlled input gain attenuation disturbance condition

Control method	$\max\|e_{sync}\|$/m	$RMSe_{sync}$/m	IAE_{sync}	$Duringmax\|e_{sync}\|$/m
IPSO-LADRC+CCC	0.012680	0.003320	0.020626	0.012613
PSO-LADRC+CCC	0.013542	0.003541	0.022384	0.013492
IPSO-LADRC	0.014375	0.003758	0.023893	0.014374
LADRC+CCC	0.020465	0.006365	0.042827	0.020465
PID+CCC	0.021852	0.006059	0.040769	0.021852

Table 9(b) Performance indices under the valve-controlled input gain attenuation disturbance condition

Control method	Recoery time/s	TV_{uL}	$RMS(u_L)'$
IPSO-LADRC+CCC	0.472	46.508	50.306
PSO-LADRC+CCC	0.395	46.881	57.343
IPSO-LADRC	0.354	48.820	75.077
LADRC+CCC	0.227	67.853	233.252
PID+CCC	0.406	80.496	341.773

Under the valve-controlled input gain attenuation disturbance condition, IPSO-LADRC+CCC obtains the smallest synchronization error indices. Its maximum synchronization error over the whole process, RMS synchronization error, and IAE are 1.2680×10^{-2}m、3.320×10^{-3}m and 2.0626×10^{-2}, respectively, all of which are lower than those of the other comparison methods. During the disturbance period, the maximum synchronization error of IPSO-LADRC+CCC is 1.2613×10^{-2}m, which is also the smallest among all methods, indicating that the proposed method can effectively suppress the dual-cylinder synchronization deviation caused by unilateral valve-controlled input gain attenuation.

Compared with PSO-LADRC+CCC, the maximum synchronization error, RMS synchronization error, and IAE of IPSO-LADRC+CCC are reduced by 6.37%, 6.25%, and 7.85%, respectively, indicating that IPSO still has a better parameter optimization effect under actuator input channel disturbance. Compared with IPSO-LADRC, after CCC is introduced, the three indices are reduced by 11.79%, 11.65%, and 13.67%, respectively, indicating that cross-coupling compensation can further improve the dual-cylinder synchronization performance under valve-controlled input disturbance.

Compared with LADRC+CCC and PID+CCC, the synchronization error advantage of IPSO-LADRC+CCC is more obvious. Its maximum synchronization error is reduced by 38.04% and 41.98%, respectively, and its RMS synchronization error is reduced by 47.84% and 45.20%, respectively. Meanwhile, the total variation of the left valve signal and the RMS of its rate of change of IPSO-LADRC+CCC are both the smallest, indicating that it does not introduce severe valve control signal fluctuations while reducing the synchronization error. Although LADRC+CCC has a

shorter recovery time, its synchronization error peak is obviously larger. Therefore, the disturbance rejection effect cannot be evaluated only according to the recovery time. Overall, IPSO-LADRC+CCC has better synchronization accuracy and control input smoothness under the valve-controlled input gain attenuation disturbance.

3.4 Engineering Significance Analysis of the Synchronization Error

To further explain the engineering significance of the synchronization error of the dual hydraulic cylinders for the coordinated advancing of the temporary support device, the maximum synchronization error under the no-disturbance step condition is converted into a relative stroke error for analysis. In the simulation, the target advancing displacement is 0.8 m, and the maximum synchronization error of IPSO-LADRC+CCC under this condition is 0.006503 m. The maximum synchronization errors of PID+CCC and LADRC+CCC are 0.017402 m and 0.017005 m, respectively. Let the target advancing displacement be S, and the maximum synchronization error be $\max\left|e_{sync}\right|$. Then, the relative synchronization error can be expressed as:

$$\eta = \frac{\max\left|e_{sync}\right|}{S} \times 100\% \tag{64}$$

Taking 1% of the target stroke as the engineering reference threshold for synchronization control accuracy, the reference error corresponding to the 0.8 m stroke is 8 mm. The conversion results of the maximum synchronization error of different control methods are shown in Table 10.

Table 10 Engineering conversion of the maximum synchronization error under the no-disturbance step condition

Control method	$\max\left\|e_{sync}\right\|$ /m	$\max\left\|e_{sync}\right\|$ /mm	Relative synchronization error/%	Below the 1% stroke reference threshold
IPSO-LADRC+CCC	0.006503	6.503	0.813	Yes
IPSO-LADRC	0.006959	6.959	0.870	Yes
PSO-LADRC+CCC	0.007515	7.515	0.939	Yes
LADRC+CCC	0.017005	17.005	2.126	No
PID+CCC	0.017402	17.402	2.175	No

It can be seen from Table 10 that the maximum synchronization errors of IPSO-LADRC+CCC, IPSO-LADRC, and PSO-LADRC+CCC are all lower than 8 mm, indicating that the optimized LADRC-type control methods can control the dual-cylinder synchronization error within 1% of the target stroke. Among them, the maximum synchronization error of IPSO-LADRC+CCC is 6.503 mm, and the relative synchronization error is 0.813%, which is the lowest among all methods. In contrast, the maximum synchronization errors of LADRC+CCC and PID+CCC are both

approximately 17 mm, and their relative synchronization errors exceed 2%, indicating that although the control methods without optimized tuning can complete target displacement tracking, the motion coordination of the dual cylinders is insufficient.

From the perspective of support frame posture, asynchronization of the left and right hydraulic cylinders causes the support frame group to exhibit deflection and torsion tendencies during the advancing process. If the lateral distance between the acting points of the left and right hydraulic cylinders is B, the equivalent posture deflection angle caused by the synchronization error can be approximately expressed as:

$$\theta \approx \arctan\left(\frac{\left|e_{sync}\right|}{B}\right) \tag{65}$$

When $\left|e_{sync}\right|$ □ B it can be approximated as:

$$\theta \approx \frac{\left|e_{sync}\right|}{B} \tag{66}$$

Therefore, under the condition that the distance between the hydraulic cylinder acting points is fixed, the equivalent posture deflection angle is approximately proportional to the synchronization error. Compared with PID+CCC, IPSO-LADRC+CCC reduces the maximum synchronization error from 17.402 mm to 6.503 mm, and the equivalent posture deflection tendency is reduced by approximately 62.63%. Compared with LADRC+CCC, the equivalent posture deflection tendency is reduced by approximately 61.76%. This indicates that the proposed method not only reduces the numerical value of the synchronization error, but also helps reduce the risks of deflection, jamming, eccentric loading, and structural impact during the advancing process of the temporary support device.

4 Conclusions

To address the dual-hydraulic-cylinder synchronization error problem caused by load-side heterogeneity during the advancing process of a temporary support device in an excavation roadway, a load-side heterogeneous dual-cylinder hydraulic system AMESim/Simulink co-simulation model was established, and an IPSO-optimized LADRC+CCC dual-cylinder synchronization control method was proposed. Through comparison with PSO-LADRC+CCC, IPSO-LADRC, LADRC+CCC, and PID+CCC, the following conclusions are obtained.

(1) Load-side heterogeneity is an important factor leading to synchronization errors of the dual hydraulic cylinders of the temporary support device. Under the condition that the left and right hydraulic cylinder bodies, servo valves, basic hydraulic circuits, and equivalent masses are consistent, differences in load-side equivalent resistance and comprehensive flexible stiffness cause the left and right hydraulic cylinders to produce different displacement response characteristics, thereby causing dual-cylinder motion asynchronization. The load-side parameter sensitivity analysis

further shows that as the resistance difference and comprehensive flexible stiffness difference between the left and right branches increase, the dual-cylinder synchronization error increases overall, indicating that changes in load-side parameters directly affect the coordinated advancing performance of the dual cylinders of the temporary support device.

(2) IPSO-LADRC+CCC can effectively improve the synchronization control accuracy of the load-side heterogeneous dual-hydraulic-cylinder system. Under the no-disturbance step condition, the maximum synchronization error of IPSO-LADRC+CCC is 6.503×10^{-3}m, which is better than those of PSO-LADRC+CCC, LADRC+CCC, and PID+CCC. Taking the target advancing displacement of 0.8 m as the benchmark, its relative synchronization error is 0.813%, which is lower than the 1% stroke reference threshold. Compared with the synchronization error level of approximately 17 mm, this method can significantly reduce the risks of support frame posture deflection, local jamming, eccentric loading, and structural impact caused by dual-cylinder asynchronization, and has clearer engineering application significance.

(3) The simulation results show that IPSO-LADRC+CCC obtains relatively small synchronization errors under disturbance conditions such as sensor disturbance, valve-controlled input gain attenuation, and unilateral load abrupt change, and has good disturbance rejection synchronization control performance. Under the unilateral load abrupt-change condition, its maximum synchronization error, RMS synchronization error, and IAE are 6.499×10^{-3}m、2.010×10^{-3}m and 1.3886×10^{-2}, respectively, all of which are better than those of the other comparison methods. Under the valve-controlled input gain attenuation condition, it can also maintain a relatively smooth valve-controlled input while reducing the synchronization error. This indicates that IPSO parameter optimization can improve the adaptability of LADRC to heterogeneous loads and input channel disturbances, and cross-coupling compensation can further enhance the synchronization coordination performance of the dual cylinders.

(4) The stability and error boundedness analysis shows that under the conditions that the reference input, the total disturbance of the system, and its rate of change are bounded, and that the controller bandwidth, observer bandwidth, nominal gain of the input channel, and cross-coupling gain satisfy positive-value constraints, the LESO observation error, single-cylinder tracking error, and dual-cylinder synchronization error can all remain uniformly ultimately bounded. This study is mainly based on a co-simulation model. In future work, prototype tests of the temporary support device and structural force analysis will be combined to further verify the real-time performance, parameter adaptability, and engineering reliability of the proposed method in an actual hydraulic system.

Author Contributions: Z.N. was responsible for theoretical analysis sections; Q.Y. is responsible for data recording and analysis and paper writing; D.Y., W.W. is responsible for data checking and validation; X.Z. is responsible for the collation of articles and correction of errors. All authors have read and agreed to the published version of the manuscript.

Funding: This study was supported by the National Natural Science Foundation of China (Grant No. 52464018), the Shanxi Province Key Research and Development Program Project (No.202402150301015), the Shanxi Province Key Research and Development Program Project (No.202304290000002). and the Datong City Key Research and Development Program (No.2025002).

Institutional Review Board Statement: Not applicable

Informed Consent Statement: Not applicable

Data Availability Statement: The datasets generated and/or analysed during the current study are available from the corresponding author on reasonable request.

Competing Interests: Authors declare no competing interests

References

[1] Li R, Yuan W, Ding X, et al. Review of Research and Development of Hydraulic Synchronous Control System[J]. processes,2023,11(4).

[2] YiNan G, Zhen Z, QingYu L, et al. Decoupling-based adaptive sliding-mode synchro-position control for a dual-cylinder driven hydraulic support with different pipelines[J]. ISA transactions,2021,123 357-371.

[3] Tianbing M, Xiangxiang G, Guoyong S, et al. Research on Synchronous Control of Active Disturbance Rejection Position of Multiple Hydraulic Cylinders of Digging-Anchor-Support Robot[J]. Sensors (Basel, Switzerland),2023,23 (8).

[4] Sun C, Dong X, Li J. Cross-Coupled Sliding Mode Synchronous Control for a Double Lifting Point Hydraulic Hoist[J]. Sensors,2023,23 (23).

[5] Zhang Z, Liu Y, Bo L, et al. Enhanced path tracking control of hydraulic support pushing mechanism via adaptive sliding mode technique in coal mine backfill operations [J]. Heliyon,2024,10 (19): e38437-e38437.

[6] Wang Y, Zhao J, Zhang H, et al. An Output Cooperative Controller for a Hydraulic Support Multi-Cylinder System Based on Neural Network Compensation[J]. Mathematics,2024,12 (12):1866-1866.

[7] Zhang F, Wang Z, Zhang X, et al. Research on Inertial Force Suppression Control for Hydraulic Cylinder Synchronization of Shield Tunnel Segment Erector Based on Sliding Mode Control[J]. Actuators,2025,14 (9):449-449.

[8] Du H, Wu Y, Zhang Z, et al. Multi - cylinder leveling control systems based on dual-valve parallel and adaptive eccentric torque suppression[J]. Mechatronics,2024,104 10 3269-103269.

[9] Zhang L, Wang J. Synchronous control of multiple hydraulic cylinders in aerial building machine using improved deep reinforcement learning[J]. Automation in Construction,2025,179 106448-106448.

[10] Chungeng S, Ruibo Y. Adaptive robust cross-coupling position synchronization control of a hydraulic press slider-leveling[J]. Science Progress,2021,104 (1):00368504209870 37-00368504209870 37.

[11] K. Li and Y. Feng, "Stabilization of T-S Fuzzy Nonlinear Systems by Intermittent Co ntrol," *2023 IEEE International Conference on Mechatronics and Automation (ICMA)*, Harbin, Heilongjiang, China, 2023, pp. 749-753.

[12] Cong X, Xiao X, Zhao L, et al. Research on multi-cylinder synchronous control syste m of multi-directional forging hydraulic press[J]. Journal of Physics: Conference Serie s,2022,2338 (1).

[13] Kunshan J, Jianli S, Yongtang L, et al. Linear active disturbance rejection control for the electro-hydraulic position servo system[J]. Science Progress,2021,104 (1):00368504 211000907-00368504211000907.

[14] Wang, L, Zhao D, Zhang Z. et al. Model-free linear active disturbance rejection outp ut feedback control for electro-hydraulic proportional system with unknown dead-zone. IET Control Theory Appl. 15, 2081–2094 (2021).

[15] Hung M N, Vu H D, Kwan K A. Active Disturbance Rejection Control for Position Tracking of Electro-Hydraulic Servo Systems under Modeling Uncertainty and Externa l Load[J]. Actuators,2021,10 (2):20-20.

[16] Bingwei G, Hao G, Wei S, et al. Application of the Gray Wolf Optimization Algorit hm in Active Disturbance Rejection Control Parameter Tuning of an Electro-Hydraulic Servo Unit[J]. Machines,2022,10 (8):599-599.

[17] Zhang J, Lu B, Chen C, et al. A New Active Disturbance Rejection Control Tuning Method for High-Order Electro-Hydraulic Servo Systems[J]. Actuators,2024,13 (8):296-296.

[18] Meng Wang, Hushan Li, Youshan Gao and et al. Active Disturbance Rejection Decou pling Control for Independent-Metering Electro-Hydraulic System With Online Compe nsation Information. IEEE Access IEEE Access, 2023, 11: 121539–121555.

[19] Yukun Z, Ruyue S, Fengming L, et al. Parameter identification and position control f or helical hydraulic rotary actuators based on particle swarm optimization[J]. Mechatro nics,2023,94.

[20] He J, Zhou L, Li C, Li T, et al. Control strategy of hydraulic servo control systems based on the integration of soft actor-critic and adaptive robust control. IEEE Access, 12: 63629–63643(2024). doi:10.1109/ACCESS.2024.3396283.

[21] Hu H, Zhang Q, Fang J, et al. Practical adaptive robust tracking control of the dual-valve parallel electro-hydraulic servo system with reduced-order model[J]. Transactions of the Institute of Measurement and Control,2024,46 (3):501-512.

[22] Dai J, Xu H, Si L, et al. Research on Feedforward-Feedback Composite Anti-Disturb

ance Control of Electro-Hydraulic Proportional System Based on Dead Zone Compens ation[J]. Machines,2024,12 (12):855-855.

[23] Pan, C.; Wang, Y.; Yang, S.X.; Li, Z.; Xiao, J. Compensation Function Observer-Base d Backstepping Sliding-Mode Control of Uncertain Electro-Hydraulic Servo System. Machines 2024, 12, 719.

[24] Zhuang H, Sun Q, Chen Z. Sliding mode control for electro-hydraulic proportional di rectional valve-controlled position tracking system based on an extended state observe r. Asian J Control. 2021; 23: 1855–1869.

[25] HAN Jinqing. Auto Disturbances Rejection Control Technique. [J]. Frontier Science. 2 007, (01): 24-31.

[26] SHAO Liwei, LIAO Xiaozhong, XIA, Qingyuan, et al. Stability Analysis and Synthes is of Third Order Discrete Extended State Observer. [J]. Information and Control. 200 8, (02): 135-139.